CHALMERS

Suspension Steady-State Kinematics and Compliance Analysis Based On Linear Bushing Model

Master's thesis in Automotive Engineering

ABHISHEK BALAKRISHNA BHAT
AKSHAY NAIK

Department of Mechanics and Maritime Sciences
CHALMERS UNIVERSITY OF TECHNOLOGY
Göteborg, Sweden 2020

MASTER'S THESIS IN AUTOMOTIVE ENGINEERING

Suspension Steady-State Kinematics and Compliance Analysis Based On Linear Bushing Model

ABHISHEK BALAKRISHNA BHAT
AKSHAY NAIK

Department of Mechanics and Maritime Sciences
Division of Vehicle Engineering and Autonomous Systems
CHALMERS UNIVERSITY OF TECHNOLOGY

Göteborg, Sweden 2020

Suspension Steady-State Kinematics and Compliance Analysis Based On Linear Bushing Model
ABHISHEK BALAKRISHNA BHAT
AKSHAY NAIK

Suspension Steady-State Kinematics and Compliance Analysis Based On Linear Bushing Model

Academic Supervisor:
Ingemar Johansson
Professor of the Practice, Vehicle Engineering and Autonomous Systems
Department of Mechanics and Maritime Sciences
Chalmers University of Technology

Examiner and Academic Supervisor:
Bengt J H Jacobson
Professor and Group leader-Vehicle Dynamics
Department of Mechanics and Maritime Sciences
Chalmers University of Technology

Industrial Supervisor:
Yansong Huang
Mechanical Systems Architect, Suspension Architecture and Structure
Wheel Suspension, Volvo Car Corporation

Master's thesis 2020:58
Department of Mechanics and Maritime Sciences
Division of Vehicle Engineering and Autonomous Systems
Chalmers University of Technology
SE-412 96 Göteborg
Sweden
Telephone: +46 (0)31-772 1000

Cover:
Volvo XC90 - Integral Suspension

Chalmers Reproservice
Göteborg, Sweden 2020

Suspension Steady-State Kinematics and Compliance Analysis Based On Linear Bushing Model
Master's thesis in Automotive Engineering
ABHISHEK BALAKRISHNA BHAT
AKSHAY NAIK
Department of Mechanics and Maritime Sciences
Division of Vehicle Engineering and Autonomous Systems
Chalmers University of Technology

Abstract

The tuning of a suspension system involves balancing various parameters and demands. There is a need for analytical tools to get a better understanding of the suspension system and to speed up the design process. In the current thesis work, an analytical tool is developed and a methodology is established to understand the effect of elastic elements like bushings and springs on kinematic and compliance parameters. The tool will also later help in choosing optimum values of bushing stiffness in order to meet the required kinematic and compliance targets.

In the first step, the position constraints and force constraints of the 5 link suspension system are modelled along with bushing elements. The bushings are modelled as a tensor with the possibilities of adjusting the bushing orientation. By using Newton Forward Euler method and non linear solver, the static equilibrium of the system at a corresponding wheel force input can be determined. This also includes the movement of the hardpoints in the suspension system during jounce, rebound and steering motions. Further the methodology is implemented to a Four link suspension and an Integral link suspension.

Sensitivity analysis is another important application of the tool. The system comprises of many bushings and sensitivity analysis is performed to understand the contribution of each bushing for a particular design parameter like toe change, camber change, brake steer, lateral force steer and so on. For the sensitivity analysis, the non linear system is linearized at small displacements and a governing equation is formulated. The governing equation consists of the stiffness matrix to map the effects of the elastic elements in the system and the constraint Jacobian to describe the velocity constraints of the system.

The process of tuning is further optimized with the help of multi-objective optimization techniques. In order to meet design targets, the process of changing the bushing stiffness individually can be time consuming. With the help of the optimization tool, the optimum values of the bushing stiffness to meet the kinematic targets can be calculated automatically based on the required wheel motion. This will save significant time during the tuning process. In order to corroborate the established methodology, the mathematical models are later verified with multi body dynamics simulation software MSC ADAMS Car. It is found that the results from the developed mathematical models have a very good match with results from MSC ADAMS Car. The developed methodology has been successfully implemented for a Five link, Four link and an Integral link suspension system. The tool also has a wide range of applications.

Keywords: Five link suspension, Integral link suspension, Four link suspension, Elastokinematic analysis, Non linear solver, Bushing optimization, Force distribution, Multi-body dynamics simulation

Acknowledgements

This thesis work has been an enriching learning experience and an opportunity to delve in depth on wheel suspensions systems. We would like to thank Volvo Cars for providing us an opportunity to conduct this thesis work. We are grateful to all our supervisors, colleagues, Chalmers University and Volvo Cars for constantly supporting us.

We would like to thank our academic supervisor at the Department of Mechanics and Maritime Sciences, Prof. Ingemar Johansson and Prof. Bengt Jacobson, Division of Vehicle Engineering and Autonomous Systems at Chalmers University of Technology for motivating us, continuously supporting and guiding us during the course of this thesis work. We would also like to thank our industrial supervisor Yansong Huang, Chassis structure and architecture design engineer in the Wheel Suspension System Architecture Department at Volvo Cars for providing us a great opportunity to work on this thesis work. We are grateful for his guidance, support on a daily basis for solving various challenging tasks in this thesis work and for sharing his valuable knowledge and experience.

We would like to thank Tobias Brandin, Daniel Molin and Benny Noren for giving us this opportunity, helping and supporting us during this thesis work. We would also like to thank other members of the wheel suspension system architecture team at Volvo Cars for giving us feedback and constantly motivating us.

Nomenclature

Symbols and Abbreviations

A_j	Transformation matrix
$\hat{b}_{ij}$	Direction vector between wheel-carrier hardpoints
d_{i-j}	Distance between hardpoints i & j [mm]
$\hat{d}_i$	Direction vector between subframe and wheel-carrier hardpoints
F_0	Force vector (F_x, F_y, F_z) [N]
J	Jacobian matrix
K and C	Kinematic and compliance
k_R	Bushing rotation stiffness [N/(mm.rad)]
K_s	Spring stiffness [N/mm]
k_T	Bushing translation stiffness [N/mm]
LCA	Lower Control Arm
λ	Lagrange multiplier
m	Distance between hardpoints P6 & P56 [mm]
M_0	Moment vector (M_x, M_y, M_z) [N/mm]
n	Distance between hardpoints P6 & P4 [mm]
ϕ	Rotation angle about x-axis [rad]
ψ	Rotation angle about z-axis [rad]
R	Rotation matrix
R_y	Steering Input [mm]
s	Spring deformation [mm]
s_x	Bushing deformation in x-direction [mm]
s_y	Bushing deformation in y-direction [mm]
s_z	Bushing deformation in z-direction [mm]
θ	Rotation angle about y-axis [rad]
UCA	Upper Control Arm

Contents

List of Figures

List of Tables

1 Introduction

1.1 Background and Problem Description

The process of development of wheel suspension in vehicles is time consuming since a lot of requirements needs to be considered and balanced. When a design proposal is ready, it is checked if all the kinematic and compliance requirements are met. The suspension attributes need to be quantified and methodologies are to be investigated to tune attributes under certain simplified assumptions. The hardpoints and bushing compliance tuning needs to be done to meet the vehicle dynamics, ride comfort, NVH and the durability attribute targets. To narrow down the tuning scope, a new method to develop the kinematics and the compliance will be developed in this thesis project.

In the early stage, hardpoints and bushing compliance are the main tuning parameters to test the kinematic/elasto-kinematics and packaging. The new method proposed in this thesis can calculate the loads and the deflections in each suspension joint and as a result of that, it is possible to predict if the suspension system meets the attribute targets, so that the engineers can understand the change from kinematic and compliance requirements perspective when they are tuning the kinematics and packaging. The complete simulation of suspension will later be more effective because of the well-defined initial tuning.

1.2 Objectives

The thesis aims to develop a methodology for kinematics and compliance tuning with the help of analytical methods. The new methodology will calculate the force and predict motion of the suspension links and bushings based on steady-state assumptions. The kinematics will be modelled with bushings. Later, various analysis like sensitivity analysis will be performed. The simulations of the suspension system to check if it meets its attribute targets on tools like MSC ADAMS Car can be time consuming. With the help of the developed tool in the current thesis work, it is possible to narrow down the design variables in kinematics and suspension bushing design.

1.3 Methodology

The following methodology will be followed during the course of this thesis work.

- Literature survey
- Mathematical modelling of suspension kinematics including bushing elements for five link suspension system
- Sensitivity analysis to understand which parameter has the highest influence on a particular kinematic and compliance property
- Mathematical modelling for integral link and four link suspension system
- Comparing the results of integral link suspension model, five link suspension model and four link suspension model with MSC ADAMS Car model

1.4 Deliverables

The main deliverables of the thesis are as given below:

- A methodology to predict the force distribution in the suspension systems
- A linear bushing model for simulation
- An observation tool to calculate wheel motion and bushing compliance
- Guidelines for bushing specifications through sensitivity analysis
- Investigate the relationship between system targets and design parameters
- Description of how the new method improves the development process

1.5 Limitations

This section focuses on the possible limitations of the current thesis work.

- The focus will be on steady-state kinematics and compliance and this project will treat the dynamic modelling as an optional research topic
- The methodology is based on a linear bushing model

2 Theory

The current section describes in depth about the theory used to develop the elasto-kinematic analysis tool. This involves topics on modelling of rigid bodies, suspension movement and methodology for linearizing a constrained mechanical system.

2.1 Five Link Suspension System

The five-link suspension is an independent type of multilink suspension system. This suspension is widely used in a modern car for their good performance and cost. The design of the five-link suspension is derived from the double wishbone suspension system. The upper and the lower wishbones are split into two-point separate links. The idea of multilink suspensions is to use several links to ensure better control and tuning of the kinematic parameters.

Due to larger number of design parameters, it has the capability of fulfilling both complex kinematic and dynamic requirements imposed on the suspension systems. It is however, more difficult to integrate than any other suspension mechanisms, due to its general spatial configuration. In case of multilink front suspension, the design problem is even more complex due to the fact that the kingpin is virtual, corresponding to the momentary screw axis of the wheel carrier performing the steering motion relative to the chassis.

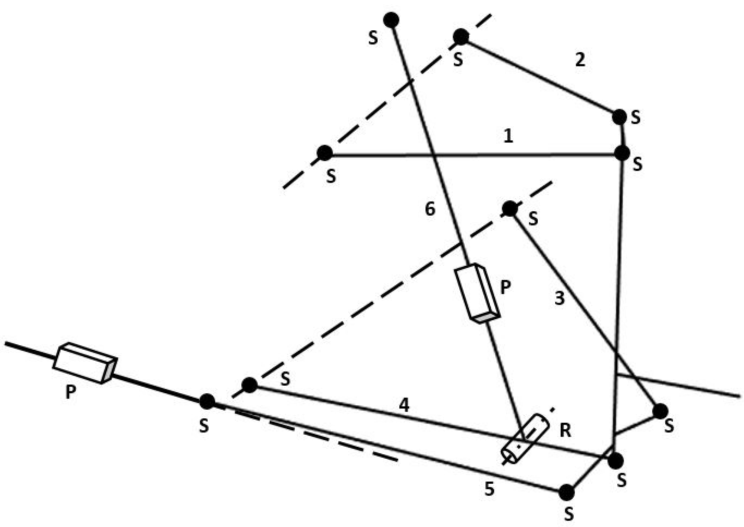

Figure 2.1: Wireframe model of a Five-Link front suspension system [6]

Commonly, these suspensions are used on a unibody vehicle which makes the subframe to be mandatory. The subframe is attached to the unibody through bushings to reduce the transmission of noise and vibrations from the wheel to the body. In the figure 2.1, link 1 and link 2 are the upper control arms, Link 3 and 4 are the lower control arms. The link arms are connected to the knuckle with spherical joints. The spring damper is mounted on the link 4 and the movement of the spring is defined with prismatic joint along link 6 and a revolute joint whose axis is perpendicular to link 4. The other end of the spring and damper is fixed to the chassis with a spherical joint. The steering input is provided by describing a prismatic joint between the rack and the chassis mounting point.

2.2 Integral Link Suspension

Another form of the multilink suspension is the Integral link suspension. The suspension system comprises of a toe link to control the toe angle change and a camber link to control the camber angle change. What makes it unique is the presence of the trapezoidal shaped lower platform which poses a challenge in modelling the suspension system. The degree of freedom for the integral link is constrained as follows:

- Two point link constrains one degree of freedom. Thus, the toe and camber link each constrain 1 DoF
- The lower platform is a special case since it is connected to the integral link. This system constrains 3 DoF

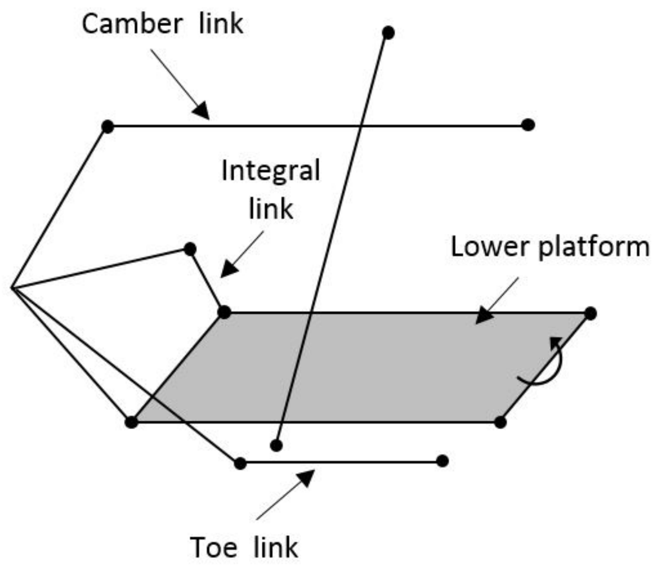

Figure 2.2: Wireframe model of an Integral link suspension system

The integral link helps to control the torques on the knuckle during acceleration and braking and thus provides a high windup stiffness. The integral link suspension can be quite complex to understand and tuning the system can be difficult.

2.3 Four Link Suspension

The four link suspension system is similar to the double wishbone suspension system. The upper control arm is common in both the systems but the lower control arm is split into two separate two point links in this system. The degree of freedom is constrained as follows:

- Each two point link constrains one degree of freedom. Thus, 3 links constrain 3 DoF
- The upper control arm constrains 2 DoF

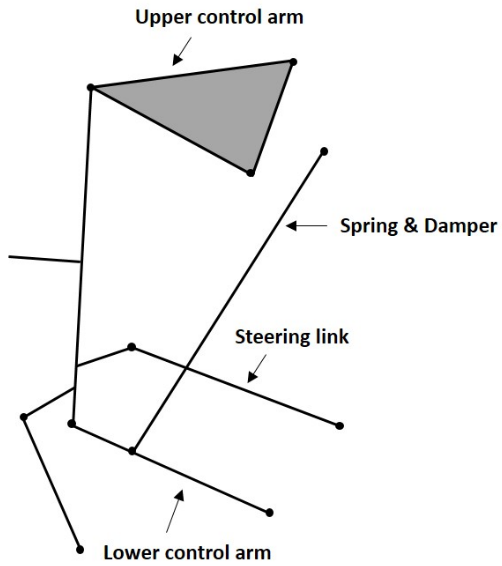

Figure 2.3: Wireframe model of a Four link suspension system

This suspension system can be more compact than a double wishbone system and makes it easier for Ackermann tuning.

2.4 Background on analytical methods for suspension kinematic analysis

There is significant research done in the areas of kinematic and compliance analysis of suspension systems. The literature review during the current thesis work has provided significant insights on the analytical methods used for the above mentioned analysis.

The paper by [1] explains the methodology used for kinematic and compliance analysis in a 5 link suspension. Here, the suspension model is only considered for one wheel in the beginning with an assumption that the masses of the links are negligible and all joints are rigid. The link elasticity is neglected and only spring and bushing elasticities are considered. For a given suspension configuration the wheel carrier equilibrium is found out by solving vectorial force and moment equations along with position constraint equations [1]. A linear spring (exerts constant force increase per deformation) is implemented and is defined as a non linear problem:

$$f(s) = R_c(s) - K_s \cdot s \tag{2.1}$$

where R_c is the spring reaction force to a wheel force input, K_s is the spring stiffness, f(s) is the constraint equation and s is the spring deformation due to a wheel force input. The above non linear problem is then solved using Newton-Raphson Method [1]. In the next step, a simple bushing model is used where a bushing is implemented only along the link direction.

However, a different approach is used in paper [2]. This paper considers a system's equilibrium in which the external forces acting on it are opposed by the internal reaction forces and elastic forces. The constraints are represented by a Jacobian which is a matrix defining the velocity constraints of the system. Based on the above equations, a governing equation is formulated, which represents a linearized system. Here, a stiffness matrix captures the elastic components in the system. The bushings are represented as a tensor, which enables the design engineer to define both translation and rotation stiffness properties. With the help of the linear governing equation, it is possible to find the different body displacements corresponding to a particular wheel force. Later, optimization techniques are used to find optimum values of bushing stiffness needed in order to meet certain kinematic and compliance parameters.

This thesis work incorporates some methodologies from the above mentioned papers in developing an analytical tool for suspension kinematic and compliance analysis using a linear bushing model. The section below describes in depth, the theoretical concepts used in the development of the analytical tool.

2.5 Local and Global Coordinate Systems

In general, global coordinate system is an absolute reference frame and is used to define the coordinate locations of points in space. All positions and orientations of different elements in the system can be defined with respect this global coordinate which is fixed in space. Whereas, the local coordinate system is a reference frame focused on a particular element of the body and the origin of this coordinate system is located within the element to simplify the algebraic computations. The local coordinate system moves with the body since it is attached to it.

When creating a local coordinate system mathematically, 3 points or markers can be used as reference. A local coordinate system consists of 3 unit vectors defined in the 3 axes. The following steps can be followed to create a local coordinate system at a point:

- First, 2 points are considered and the unit vector 'p' between the 2 points is determined
- With one of the above used points as reference, a third point which is perpendicular to it is defined and the unit vector 'q' between them is calculated
- The cross product of the unit vectors 'p' and 'q' will give the third unit vector 'r' which is perpendicular to the above two unit vectors. The direction of the cross product can be found out with the help of the right hand rule

These 3 unit vectors when arranged in a matrix form will give the rotation matrix. This rotation matrix describes the orientation of the local coordinate system with respect to another coordinate system.

In the figure 2.4, the orientation of the local coordinate system is same as the global coordinate system, thus the rotation matrix describing the orientation of the local coordinate system to the global coordinate system can be represented by a 3x3 identity matrix.

Consider G as the global coordinate system and L as the local coordinate system at (x_1, y_1, z_1)

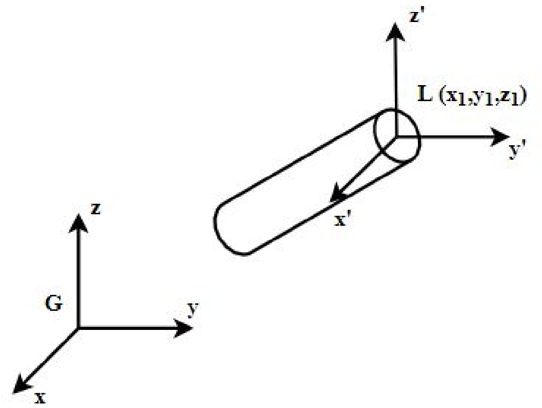

Figure 2.4: Global and Local Coordinate systems

from G. The relation between these two coordinate systems can be expressed by a transformation matrix [6]. This matrix denotes the location and orientation of the local frame or an element with respect to a particular coordinate system.

$$T_L^G = \begin{bmatrix} R_L^G & O_L^G \\ 0_{1\times3} & 1 \end{bmatrix}$$

Where R_L^G is the rotation matrix and represents the orientation of the frame L with respect to frame G. O_L^G represents the position of L with respect to G frame.

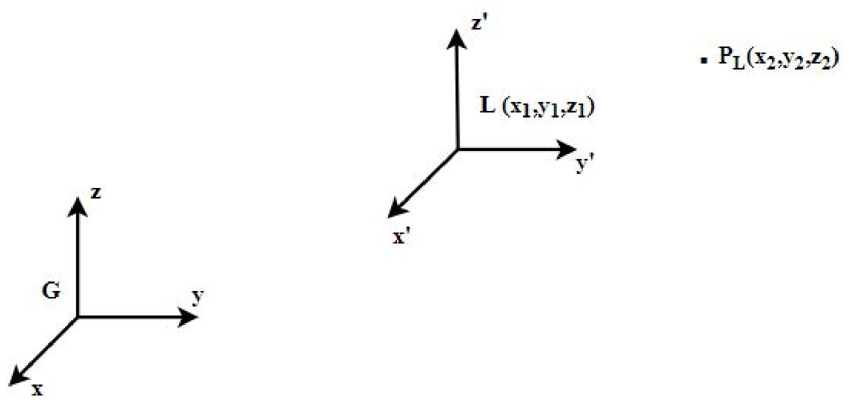

Figure 2.5: Transformation from one coordinate to another coordinate system

Consider a point $P_L(x_2, y_2, z_2)$ with respect to local coordinate system. If this point needs to be expressed in global coordinate system, it can be represented as shown below [6].

$$P_G = L + R_L^G \cdot P_L \tag{2.2}$$

$$P_G = \begin{bmatrix} x_1 \\ y_1 \\ z_1 \end{bmatrix} + \begin{bmatrix} 1 & 0 & 0 \\ 0 & 1 & 0 \\ 0 & 0 & 1 \end{bmatrix} \cdot \begin{bmatrix} x_2 \\ y_2 \\ z_2 \end{bmatrix} \tag{2.3}$$

Since the orientation of frame L is same as global reference G, the rotation matrix is an identity matrix. Then point P with global reference will be:

$$P_G = [(x_1 + x_2), \ (y_1 + y_2), \ (z_1 + z_2)]$$

2.6 Describing orientations of a rigid body

The orientation of a rigid body can be represented by using different methods. In the current thesis work we will discuss about Euler angles and Quaternion forms for describing orientations. For a given rigid body, the orientations of different points on the body can be determined with the help of a single local coordinate system on the body.

2.6.1 Euler Angles

The Euler angles are a simple way of representing body orientation. In this method, 3 angles are used to denote the orientation of a body with respect to a particular coordinate system. For example, let Euler angles ϕ, θ and ψ denote the orientation of a local coordinate system with respect to the global coordinate system. The local coordinate system would align with global coordinate system if it is rotated by the above three Euler angles in a particular sequence.

The angles ϕ, θ and ψ are the rotation angles about x, y and z axes respectively. The rotations are considered according to the right hand rule. The rotation matrix for rotation about each axis is given as follows [7].

$$R_x(\phi) = \begin{bmatrix} 1 & 0 & 0 \\ 0 & cos(\phi) & -sin(\phi) \\ 0 & sin(\phi) & cos(\phi) \end{bmatrix} R_y(\theta) = \begin{bmatrix} cos(\theta) & 0 & sin(\theta) \\ 0 & 1 & 0 \\ -sin(\theta) & 0 & cos(\theta) \end{bmatrix} R_z(\psi) = \begin{bmatrix} cos(\psi) & -sin(\psi) & 0 \\ sin(\psi) & cos(\theta) & 0 \\ 0 & 0 & 1 \end{bmatrix}$$

Different conventions can be derived from these three matrices. For example in the case of Z-Y-X, the rotation sequence is rotation ψ about z-axis then rotation θ about y-axis and finally, rotation ϕ about x-axis. The combined rotation is given by [7],

$$R_z(\psi)R_y(\theta)R_x(\phi) =$$
$$\begin{bmatrix} cos\psi \cdot cos\theta & cos\psi \cdot sin\theta \cdot sin\phi - sin\psi \cdot cos\phi & cos\psi \cdot sin\theta \cdot cos\phi + sin\psi \cdot sin\phi \\ sin\psi \cdot cos\theta & sin\psi \cdot sin\theta \cdot sin\phi + cos\psi \cdot cos\phi & sin\psi \cdot sin\theta \cdot cos\phi - cos\psi \cdot sin\phi \\ -sin\theta & cos\theta \cdot sin\phi & cos\theta \cdot cos\phi \end{bmatrix}$$

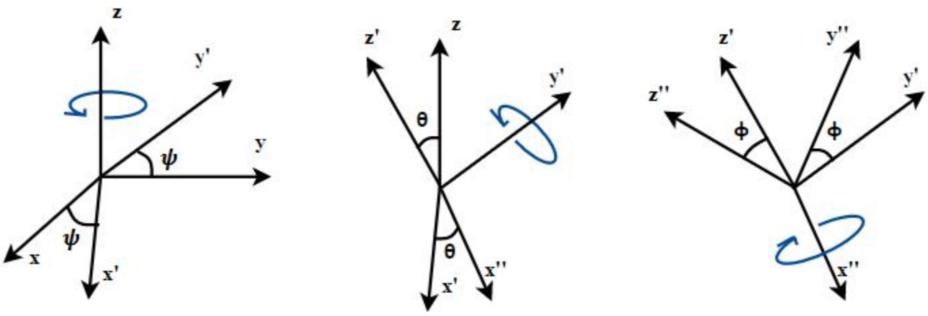

Figure 2.6: ZYX transformation

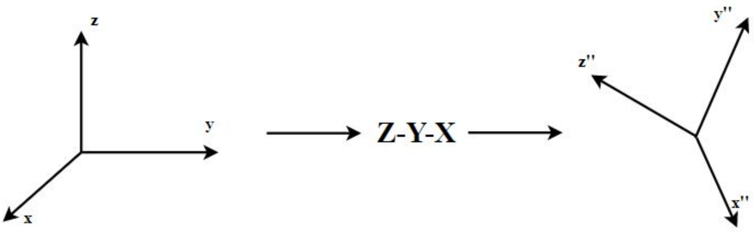

Figure 2.7: Change in Orientation due to ZYX convention

There are different sequence of rotations of Euler angles which can be used. When the sequence of rotation changes, the rotation matrix will also change accordingly.

There is one limitation of using Euler angles known as 'Gimbal Lock'. Under certain body rotations there are cases when one degree of freedom is lost due to any 2 axes becoming parallel to each other. This can be a problem for the numerical solver as this can lead to singularity errors. However, this singularity error can be avoided when Quaternions are used to represent body orientations.

2.6.2 Quaternions

As mentioned above, with the help of Quaternions, singularity errors in solvers can be avoided. The unit quaternions can be represented with the help of 4 parameters e_0,e_1,e_2,e_3 which help to separate the magnitude and the direction. The unit quaternions can be related to one another by the following equation [6]:

$$e_0^2 + e_1^2 + e_2^2 + e_3^2 = 1$$

The rotation matrix can also be represented in form of quaternions as follows [6]:

$$R = \begin{bmatrix} e_0^2 + e_1^2 - e_2^2 - e_3^2 & 2 \cdot (e_1 \cdot e_2 - e_0 \cdot e_3) & 2 \cdot (e_1 \cdot e_3 + e_0 \cdot e_2) \\ 2 \cdot (e_1 \cdot e_2 + e_0 \cdot e_3) & e_0^2 - e_1^2 + e_2^2 - e_3^2 & 2 \cdot (e_2 \cdot e_3 - e_0 \cdot e_1) \\ 2 \cdot (e_1 \cdot e_3 - e_0 \cdot e_2) & 2 \cdot (e_2 \cdot e_3 + e_0 \cdot e_1) & e_0^2 - e_1^2 - e_2^2 + e_3^2 \end{bmatrix}$$

The rotation matrices can be transformed from one form to another based on the method chosen for describing the body's orientation. In this thesis work, the body's orientation is described with the help of Euler angles using the ZYX convention. The rotation matrix expressed in form of Euler angles can be represented in form of quaternions with the parameters for quaternions calculated as follows [7]:

$$e_0 = sin(\psi/2) \cdot sin(\theta/2) \cdot sin(\phi/2) + \cos(\psi/2) \cdot cos(\theta/2) \cdot cos(\phi/2)$$

$$e_1 = -sin(\psi/2) \cdot sin(\theta/2) \cdot cos(\phi/2) + \sin(\phi/2) \cdot cos(\psi/2) \cdot cos(\theta/2)$$

$$e_2 = sin(\psi/2) \cdot sin(\phi/2) \cdot cos(\theta/2) + \sin(\theta/2) \cdot cos(\psi/2) \cdot cos(\phi/2)$$

$$e_3 = sin(\psi/2) \cdot cos(\theta/2) \cdot cos(\phi/2) \text{ - } \sin(\theta/2) \cdot sin(\phi/2) \cdot cos(\psi/2)$$

The above equations are useful to understand how the conversion works between different forms. However, when modelling the system in MATLAB, these conversions are easier with the help of standard syntax from the robotic toolbox. The toolbox enables conversion from Euler angles to quaternions and vice versa based on the required sequence of rotation.

2.7 Degree of freedom

A body can be described in space with the help of generalized coordinates [2]. The degree of freedom describes the number of independent coordinates required to define the configuration of a body. In an unconstrained state, a body has a total of 6 degrees of freedom in which 3 degrees of freedom are the translation in x, y, z axes and the remaining 3 DoF are the rotations along the 3 axes. The wheel movement in a vehicle is a constrained motion which depends on the type of suspension and its geometry. The suspension system consists of different links constrained to move in a particular direction with the help of joints and compliance elements like bushings. The degree of freedom of a body can be found out with the help of the mobility equation which is given by:

$$M = 6n - \Sigma_{i=1}^{j}(6 - f_i) \tag{2.4}$$

where, n is the number of moving links and j is the number of joints. The term f_i describes the degree of freedom of the joint and depends on the type of joint being used.

Few of the commonly used joints in a suspension system and their applications in modelling suspension kinematics are mentioned below [5]:

- Prismatic joint: This joint is used to describe the translation motion between two bodies and offers only one degree of freedom. This kind of joint is used when defining motion between the rack and the steering link to define a steering input to the wheel
- Spherical joint: This joint describes the rotation between two bodies and offers 3 degrees of freedom which is the rotation along the three axes. This joint does not allow any translation and is commonly used in connecting the link arms to the wheel carrier or the knuckle.

- Universal joint: The joint allows rotation between two bodies whose axis are inclined to each other. The joint arrests 4 degrees of freedom and allows rotation along the body axes which contributes to 2 Dof. In a 5 link suspension, universal joints are used to connect the link arms to the subframe.
- Revolute joint: This joint is used to describe rotation between two bodies along only one axes and offers only 1 DoF. In suspension systems like the double wishbone, the A-arms are connected to the chassis by a revolute joint.
- Cylindrical joint: The cylindrical joint allows translation and rotation between two bodies only along one axes and this joint gives only two degrees of freedom. In modeling a spring damper system (strut), a cylindrical joint can be used to describe its motion in systems like McPherson.

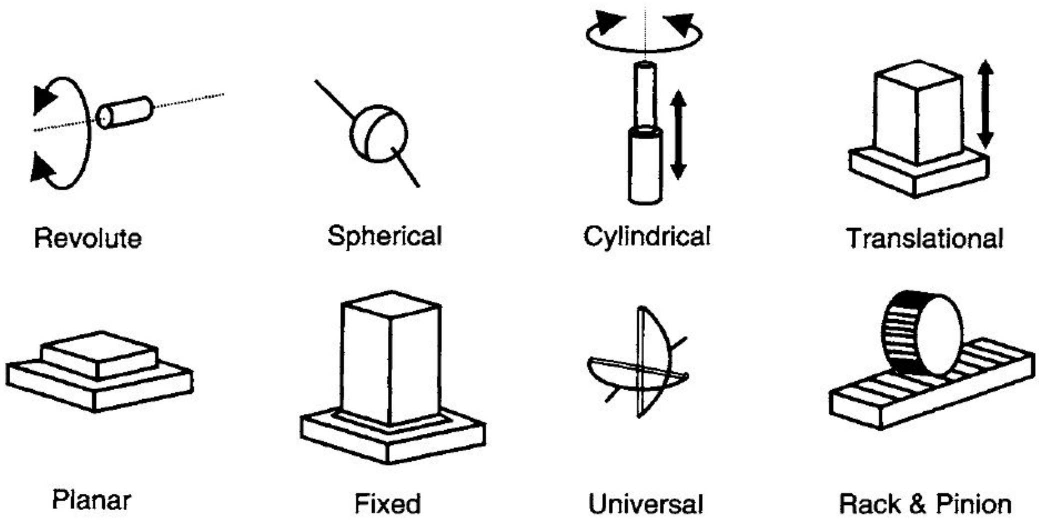

Figure 2.8: Pictorial representation of types of joints [5]

2.8 Linearized equations for a constrained mechanical system

A constrained system like a wheel suspension system can be represented by a governing equation. The governing equation is derived with the assumption that the body undergoes very small displacements. Small displacements are assumed as the system is linearized around these points. The governing equation consists of algebraic constraint equations and dynamic differential equations [4]. The kinematic constraint equations is represented as $\phi(q) = 0$, where q represents the generalized coordinates of the body [2]. The displacements of the body are represented with the help of generalized coordinates $\Delta q = [\Delta r \ \Delta\pi]$ where, Δr represents the translation movements along the three axes and $\Delta\pi$ is the rotation movement along the three axes. Since the system is linearized at small displacements [2]:

$$\phi(q + \Delta q) = 0 \tag{2.5}$$

$$\phi(\Delta q) = 0 \tag{2.6}$$

In the above equations, ϕ_q denotes the constraint jacobian. The matrix consists of partial derivatives of constraint equations and helps to capture the kinematic constraints in the system.

In simple words, the position constraints can be expressed as a function of Δq which represents body's translation and rotation movement. These constrains needs to be maintained as the body moves from one point to another.

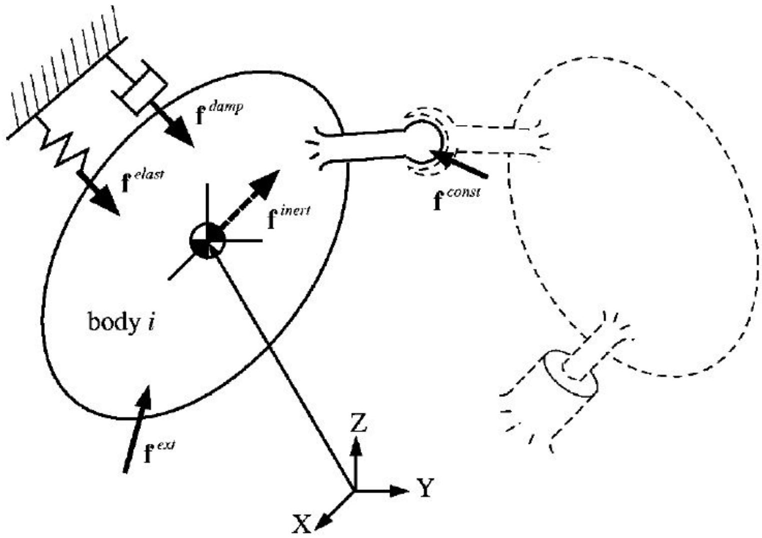

Figure 2.9: Free body diagram of bodies connected by joints, elastic elements, subjected to external forces [4]

In the figure 2.9, consider the two bodies as shown which is connected by any joint [4]. The free body diagram of the system yields the following equation [4]:

$$f^{elast} + f^{damp} + f^{inert} + f^{const} = f^{ext} \tag{2.7}$$

In the above equation,

f^{elast} - Elastic forces, contributions to these are the elastic elements in the system like springs and bushings

f^{damp} - These are the forces due to the damping elements in the system

f^{inert} - This represents the inertial forces in the system due to the mass of each component. In systems like the integral link suspension, inertial properties needs to be modelled for better fidelity. This force can be neglected in the steady state models

f^{const} - These are the constraint forces in the system due to the joint connection between two bodies

f^{ext} - The external forces acting on the system. This can be in the form of the forces at the tyre contact

In the current thesis work, the analysis is simplified by neglecting the terms associated with the damping and the inertial forces. These are important when dynamic behaviour of the system needs to be assessed. The elastic forces and the constraint reaction forces can be determined with the help of the equation [2]:

$$f^{elast} = K \cdot \Delta q \tag{2.8}$$

$$f^{const} = \phi_q^T \cdot \lambda \tag{2.9}$$

The equilibrium equation for the system is now reduced to the following:

$$K \cdot \Delta q + \phi_q^T \cdot \lambda = f^{ext} \tag{2.10}$$

In the above equations, K represents stiffness matrix and λ represents the lagrange multiplier. Based on the equation 2.10 and the equation describing the condition for kinematic constraints, the linear governing equation of the system can be formulated as follows [2]:

$$\begin{bmatrix} f^{ext} \\ 0 \end{bmatrix} = \begin{bmatrix} K & \phi_q^T \\ \phi_q & 0 \end{bmatrix} \cdot \begin{bmatrix} \Delta q \\ \lambda \end{bmatrix} \tag{2.11}$$

The governing equation is obtained by linearizing the system at small displacements and terms associated with it are described in detail below.

2.8.1 Constraint Jacobian

The constraint Jacobian is a matrix of first order partial derivatives of the constraint equations. Consider the time derivative of the constraint equation [8],

$$\frac{dF}{dt} \cdot \Delta q = \frac{dF}{dt} \cdot s \cdot \frac{d\Delta q}{dt} \tag{2.12}$$

The term $\frac{dF}{dt}.s$ is known as the jacobian and the term $\frac{d\Delta q}{dt}$ denotes the velocity. Thus the equation below represents the velocity constraint. This means that we are working on a velocity level. In order to find the positions of static equilibrium, the velocities of the bodies are computed and later the positions and orientations of the body such that all the constraints are satisfied.

$$\tfrac{dF}{dt} \cdot \Delta q = \phi_q \cdot v(t)$$

As mentioned earlier, ϕ_q is the jacobian matrix and comprises of partial derivatives. The general form of a jacobian matrix with 'm' functions and 'n' parameters can be expressed as follows:

$$\phi_q = \begin{bmatrix} \frac{\partial f_1}{\partial x_1} & \frac{\partial f_1}{\partial x_2} & \frac{\partial f_1}{\partial x_3} & \cdots\cdots & \frac{\partial f_1}{\partial x_n} \\ \frac{\partial f_2}{\partial x_1} & \frac{\partial f_2}{\partial x_2} & \frac{\partial f_2}{\partial x_3} & \cdots\cdots & \frac{\partial f_2}{\partial x_n} \\ \frac{\partial f_3}{\partial x_1} & \frac{\partial f_3}{\partial x_2} & \frac{\partial f_3}{\partial x_3} & \cdots\cdots & \frac{\partial f_3}{\partial x_n} \\ \vdots & \vdots & \vdots & \vdots & \vdots \\ \frac{\partial f_m}{\partial x_1} & \frac{\partial f_m}{\partial x_2} & \frac{\partial f_m}{\partial x_3} & \cdots\cdots & \frac{\partial f_m}{\partial x_n} \end{bmatrix}$$

2.8.2 Stiffness matrix

The stiffness matrix helps to relate the force and displacements between different bodies in a system. It includes the stiffness of the spring and bushing elements. The bushings can be represented by a tensor which helps to capture its orthotropic properties. As mentioned in the paper [2], the stiffness matrix between two bodies 'i' and 'j' can be computed by the following matrices:

$$k_{ii} = \begin{bmatrix} -k_T & k_T \cdot s_i \\ -s_i \cdot k_T & -s_i \cdot k_T \cdot s_i - k_R \end{bmatrix} \tag{2.13}$$

$$k_{ij} = \begin{bmatrix} k_T & -k_T \cdot s_j \\ s_i \cdot k_T & -s_i \cdot k_T \cdot s_j + k_R \end{bmatrix} \tag{2.14}$$

$$k_{ji} = \begin{bmatrix} -k_T & -k_T \cdot s_i \\ -s_j \cdot k_T & -s_j \cdot k_T \cdot s_i + k_R \end{bmatrix} \tag{2.15}$$

$$k_{jj} = \begin{bmatrix} -k_T & k_T \cdot s_j \\ -s_j \cdot k_T & s_j \cdot k_T \cdot s_j - k_R \end{bmatrix} \tag{2.16}$$

In the above matrices, k_T and k_R represents the stiffness matrices in the global coordinate system and are the translation stiffness and the rotation stiffness respectively. The terms s_i and s_j are the position vectors from the local coordinate systems of the body to the local coordinate of the elastic elements [2]. The stiffness matrices can be transformed from local to global coordinate as follows with the help of the transformation matrix A_j [2]:

$$k_T = A_j.k_T.A_j^T$$
$$k_R = A_j.k_R.A_j^T$$

Since the translation and rotation stiffness are defined in form of tensors, the transformation matrices are pre and post multiplied as shown above.

2.9 Non linear solver structure

In order to solve the positions of static equilibrium, the non linear solver 'fsolve' is used in MATLAB. The sequence of operations in which the non linear solver computes is indicated in the chart below.

- Initialize values: The values of the parameters which the solver iterates are initialized. These are the starting values from which the solver begins to solve the system of equations
- Position constraint: These are the set of equations defined to represent the suspension geometry and the rigid links. These constraints define how the hardpoints move with respect to one another
- Direction vectors: Once the position constraints are solved, the new position of the suspension system at that instant can be determined. The direction vectors with respect to the new points are calculated and these vectors are used in defining the direction of reaction forces in moment and force equations
- Tyre forces: These are the inputs to the system and is characterized by the wheel vertical, longitudinal, lateral loads and the wheel overturning, self aligning and the rolling resistance moment

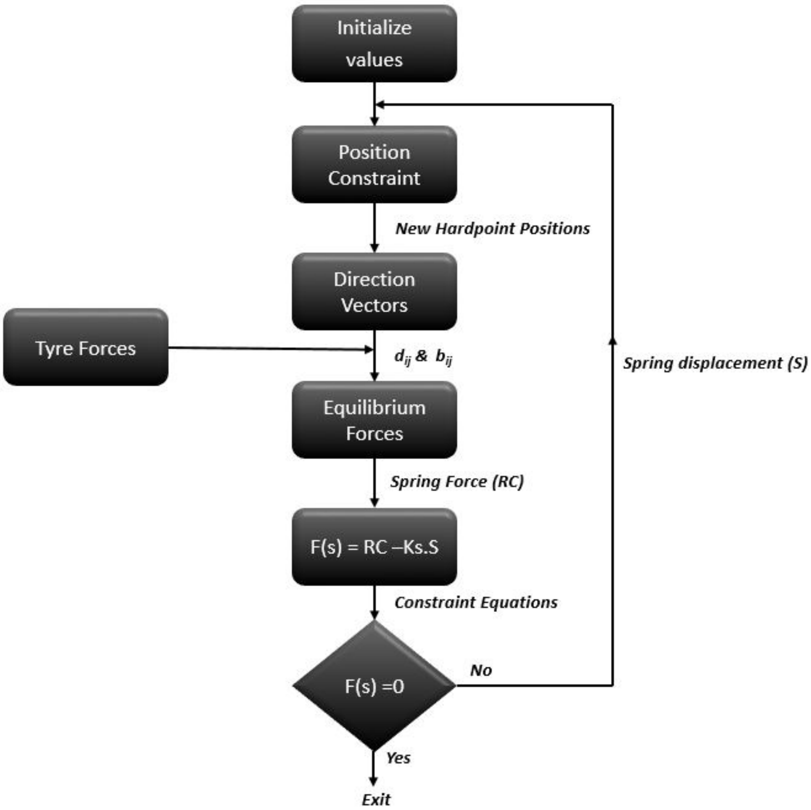

Figure 2.10: Flow diagram of the Nonlinear Solver structure

- Equilibrium forces: The reaction forces at different joints can be computed with the help of the linear force matrix or by an alternative method which will be explained in the later sections. These forces will be used as an input for the constraint equations and this will help the solver to determine the static equilibrium position
- Constraint equations: The non linear solver solves the system of position constraint and the force constraint equations till the value of the non linear function converges to zero. Once the system of equations are solved we get the final position of the suspension system, spring displacement, bushing displacement and reaction forces.

This is the structure in which the non linear solver is implemented in the current work. The above process as described in the flow diagram is an iterative method and is sensitive to the initialized values and the solver setup. The solver setup gives the possibility of choosing the algorithm, tolerance values for the functions.

3 Modelling Five Link Suspension Kinematics

The methodology for elasto-kinematic analysis is first established for a five link suspension system. Before we start with the modelling, it is important to evaluate the number of unknowns and equations. The number of unknowns need to be counted for the force matrix and for the non linear solver. In the case of the five link suspension system with bushings at the subframe side, the number of unknowns for the force matrix can be calculated as follows:

- For pure kinematic models and two point links, the line of action of force is known. Thus, there is only one force unknown at each joint. When a bushing is introduced at a joint three force unknowns are needed to model the force matrix
- For a compliant model we have, 6 force unknowns for each link. Considering four links with bushings, we have a total of 24 force unknowns.
- One force unknown for the spring system and steering link

The force matrix for the compliant model now consists of 26 unknowns and 30 equations. So we have a deficit of 4 unknown parameters.

The next step is to look at the number of unknowns in the non linear solver. The non linear solver parameters are the position (3 parameters) and translation (3 parameters) of the local coordinate systems and spring displacement. In the case of the 5 link with 4 compliance elements, we need 5 local coordinate systems to capture the suspension movement. We have one local coordinate at the wheel center and one each at the end of the link on which the bushing is mounted. Thus, the solver now has 30 unknown parameters and an additional unknown 's' to determine the spring displacement. The system currently has 31 unknowns. The possible number of equations that can be formulated are:

- Each link can be modelled with one position constraint equation. A link with bushing can be modelled with 3 position constraint equations. On the similar basis, the system has 14 position constraint equations (4 links with bushing and 1 link with kinematic joint)
- There are additional 12 equations to constrain the bushing translation displacement and one to constrain the spring displacement

There are 27 equations and 31 unknowns in the non linear solver. In order to solve this mismatch, the rotation about the link axis ζ is introduced. This results in four unknown parameters (one for each link) that can be introduced in the force matrix. Thus, the force matrix now has 30 unknowns and 30 equations. Four equations can be introduced in the non linear solver to constrain this rotation. The non linear solver will now have 31 unknowns and 31 equations. The system is now completely constrained. The mathematical modelling is divided into three main stages:

- Position constraints modelling
- Force distribution modelling
- Bushing modelling

The above mentioned parameters like ζ and the three stages of modelling will be explained in depth in the next section.

3.1 Position Constraints

To determine the position of the hardpoints after the suspension attains the static equilibrium due to a wheel force input, a mathematical model is built with a set of constraint equations which defines the movement of the suspension under the external forces.

The figure 3.1 is the basic structure of the five-link suspension system with P9 being the wheel centre and CP being the wheel road contact point. The links P1-P7 and P2-P8 form the upper control arms and the links P3-P5 and P4-P6 form the lower control arms with P14-P12 being the steering link. P55-P56 is the helical spring with spring deflection 's'. All these points are defined with respect to global coordinate system.

All the wheel Carrier hardpoints (P9, P7, P8, P5, P6, P12 & P56) are the moving hardpoints. Thus, we have a set of 21 unknowns and we need 21 equations to solve them. To make this computation easier, a local coordinate is created at the wheel centre P9 with Euler angles (ψ,θ,ϕ) of ZYX transformation. The rotation matrix is formulated using these Euler angles [7].

$$R = \begin{bmatrix} cos\psi \cdot cos\theta & cos\psi \cdot sin\theta \cdot sin\phi - sin\psi \cdot cos\phi & cos\psi \cdot sin\theta \cdot cos\phi + sin\psi \cdot sin\phi \\ sin\psi \cdot cos\theta & sin\psi \cdot sin\theta \cdot sin\phi + cos\psi \cdot cos\phi & sin\psi \cdot sin\theta \cdot cos\phi - cos\psi \cdot sin\phi \\ -sin\theta & cos\theta \cdot sin\phi & cos\theta \cdot cos\phi \end{bmatrix}$$

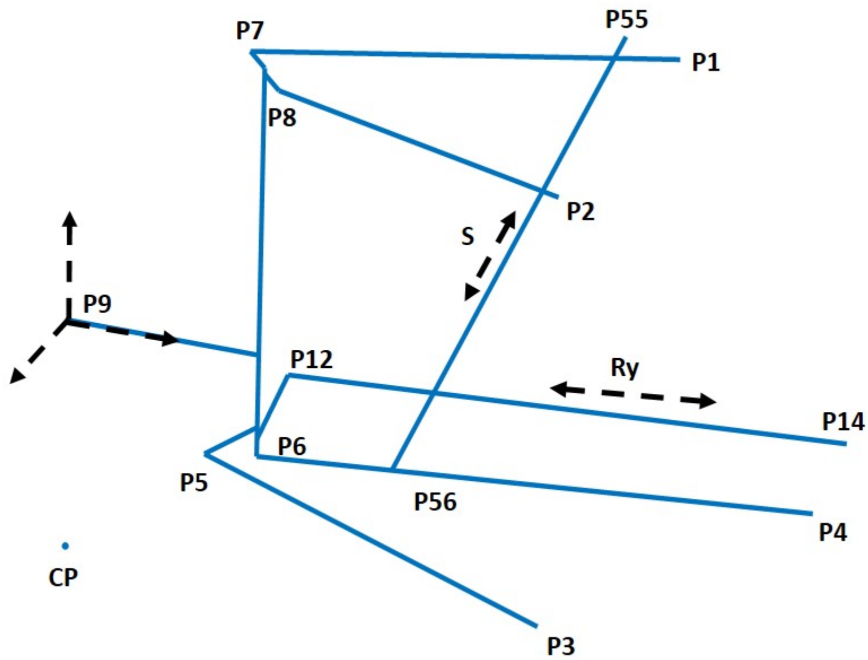

Figure 3.1: Wire frame model of a five link suspension with a local coordinate at P9

All the wheel carrier points can now be defined with respect to the local coordinate system at P9. For easier computation, the initial orientation of the local coordinate system is taken to be same as the global coordinate system, i.e Euler angles are zero.

$$R_{init} = \begin{bmatrix} 1 & 0 & 0 \\ 0 & 1 & 0 \\ 0 & 0 & 1 \end{bmatrix}$$

The wheel carrier points with respect to local coordinate system can now be defined with the help of coordinate transformations as follows,

$$P5l = \frac{R_{init}}{P5 - P9} \tag{3.1}$$

Similarly, other hardpoints on the knuckle can be defined with respect to the local coordinate at P9. The hardpoint P56 cannot be directly represented as shown above. Since it lies on the lower control arm P6-P4 and not on the knuckle, the location of P56 can be determined with respect to local coordinate system at P4 i.e

$$P56l = \frac{R_{init}}{P56 - P4} \tag{3.2}$$

Where, m is the distance between P6 and P56 and n is the distance between P56 and P4.

3.2 Constraint Equations

The following are the position constraint equations for the five link suspension system. The number of equations have been reduced to 6 with the introduction of the local coordinate system at P9. The points x_0, y_0, z_0 denote the wheel center coordinates.

Since the links are rigid in nature, the distance between points P5-P3 (d_{5-3}), P4-P6(d_{6-4}), P12-P14(d_{12-14}), P2-P8(d_{8-2}) and P7-P1(d_{7-1}) are fixed during wheel travel for pure kinematic joints. The same can be modelled with the help of distance formula as shown in the equations below.

$$\begin{aligned}
&(x_0 + R(1,1)\cdot P8l(1) + R(1,2)\cdot P8l(2) + R(1,3)\cdot P8l(3) - P2(1))^2 + \\
&(y_0 + R(2,1)\cdot P8l(1) + R(2,2)\cdot P8l(2) + R(2,3)\cdot P8l(3) - P2(2))^2 + \\
&(z_0 + R(3,1)\cdot P8l(1) + R(3,2)\cdot P8l(2) + R(3,3)\cdot P8l(3) - P2(3))^2 - d_{8-2}^2 = 0
\end{aligned} \tag{3.3}$$

$$\begin{aligned}
&(x_0 + R(1,1)\cdot P7l(1) + R(1,2)\cdot P7l(2) + R(1,3)\cdot P7l(3) - P1(1))^2 + \\
&(y_0 + R(2,1)\cdot P7l(1) + R(2,2)\cdot P7l(2) + R(2,3)\cdot P7l(3) - P1(2))^2 + \\
&(z_0 + R(3,1)\cdot P7l(1) + R(3,2)\cdot P7l(2) + R(3,3)\cdot P7l(3) - P1(3))^2 - d_{7-1}^2 = 0
\end{aligned} \tag{3.4}$$

$$\begin{aligned}
&(x_0 + R(1,1)\cdot P12l(1) + R(1,2)\cdot P12l(2) + R(1,3)\cdot P12l(3) - P14(1))^2 + \\
&(y_0 + R(2,1)\cdot P12l(1) + R(2,2)\cdot P12l(2) + R(2,3)\cdot P12l(3) - (P14(2) - Ry))^2 + \\
&(z_0 + R(3,1)\cdot P12l(1) + R(3,2)\cdot P12l(2) + R(3,3)\cdot P12l(3) - P14(3))^2 - d_{12-14}^2 = 0
\end{aligned} \tag{3.5}$$

$$\begin{aligned}
&(x_0 + R(1,1)\cdot P5l(1) + R(1,2)\cdot P5l(2) + R(1,3)\cdot P5l(3) - P3(1))^2 + \\
&(y_0 + R(2,1)\cdot P5l(1) + R(2,2)\cdot P5l(2) + R(2,3)\cdot P5l(3) - P3(2))^2 + \\
&(z_0 + R(3,1)\cdot P5l(1) + R(3,2)\cdot P5l(2) + R(3,3)\cdot P5l(3) - P3(3))^2 - d_{5-3}^2 = 0
\end{aligned} \tag{3.6}$$

$$
\begin{aligned}
&(x_0 + R(1,1) \cdot P6l(1) + R(1,2) \cdot P6l(2) + R(1,3) \cdot P6l(3) - P4(1))^2 + \\
&(y_0 + R(2,1) \cdot P6l(1) + R(2,2) \cdot P6l(2) + R(2,3) \cdot P6l(3) - P4(2))^2 + \\
&(z_0 + R(3,1) \cdot P6l(1) + R(3,2) \cdot P6l(2) + R(3,3) \cdot P6l(3) - P4(3))^2 - (d_{6-4})^2 = 0
\end{aligned} \tag{3.7}
$$

The distance between points P55 and P56 is controlled by the spring displacement 's'.

$$
\begin{aligned}
&(P4_x + R_4(1,1) \cdot P56l(1) + R_4(1,2) \cdot P56l(2) + R_4(1,3) \cdot P56l(3) - P55(1))^2 + \\
&(P4_y + R_4(2,1) \cdot P56l(1) + R_4(2,2) \cdot P56l(2) + R_4(2,3) \cdot P56l(3) - P55(2))^2 + \\
&(P4_z + R_4(3,1) \cdot P56l(1) + R_4(3,2) \cdot P56l(2) + R_4(3,3) \cdot P56l(3) - P55(3))^2 \\
&- (d_{56-55} - s)^2 = 0
\end{aligned} \tag{3.8}
$$

These six equations are used to trace the position of the wheel carrier hardpoints with spring deflection 's' and steering rack travel 'Ry' as inputs to position constraints nonlinear solver. These nonlinear equations are solved for x0, y0, z0, ϕ, θ and ψ. The obtained values are position and orientation of the local coordinate located at P9. The other hardpoints are calculated and transformed back to global coordinates system as follows.

$$
P5n = \frac{R_{init}}{R \cdot (P5 - P9) + R_{init} \cdot P9n} \tag{3.9}
$$

Similarly, P6n, P7n, P8n & P12n can be calculated.

$$
P56n = \frac{R_{init}}{R_4 \cdot (P56 - P4) + R_{init} \cdot P4} \tag{3.10}
$$

To find the wheel contact point, the toe angle and the camber angle can be used. As the wheel starts to move, the toe and the camber angle changes due to the kinematic constraints of the suspension system.

A point P21 is selected along the knuckle and wheel center line. As the wheel moves under a certain force input, new equilibrium position is achieved and the new position of P21 is calculated with respect to P9.

The toe and camber angles are then be calculated by:

$$
toe_{angle} = \sin^{-1}\left(\frac{(P21_x - P9_x)}{\sqrt{(P21_x - P9_x)^2 + (P21_y - P9_y)^2}}\right) \tag{3.11}
$$

$$
camber_{angle} = \sin^{-1}\left(\frac{(P21_z - P9_z)}{\sqrt{(P21_x - P9_x)^2 + (P21_y - P9_y)^2 + (P21_z - P9_z)^2}}\right) \tag{3.12}
$$

The contact point(CP) is determined with the help of toe and camber angles as,

$$
CP = P9 + Radius_{Wheel} \begin{bmatrix} -\sin(camber) \cdot \sin(-toe) \\ \sin(camber) \cdot \cos(toe) \\ -\cos(camber) \end{bmatrix} \tag{3.13}
$$

The computed toe and camber angles are important to understand the change in kinematic parameters under various wheel loads. These parameters will also play a key role in multi objective optimization and will be explained in depth in the later sections.

3.3 Force Equilibrium

The position constraint model allows to track the wheel center movement for a particular value of spring deflection. However, the inputs to the entire system are the forces acting at the wheel contact point and the steering rack travel. The steering input can be included in the position constraint equations to find the new equilibrium position. However, the spring deflection needs to be calculated first (calculated by the solver), corresponding to the applied wheel forces and can later be used to solve the position constraint equations. Before formulating the force equilibrium equations, it is important to count the number of unknown forces and equations in the system. This is done to check if the system is completely constrained.

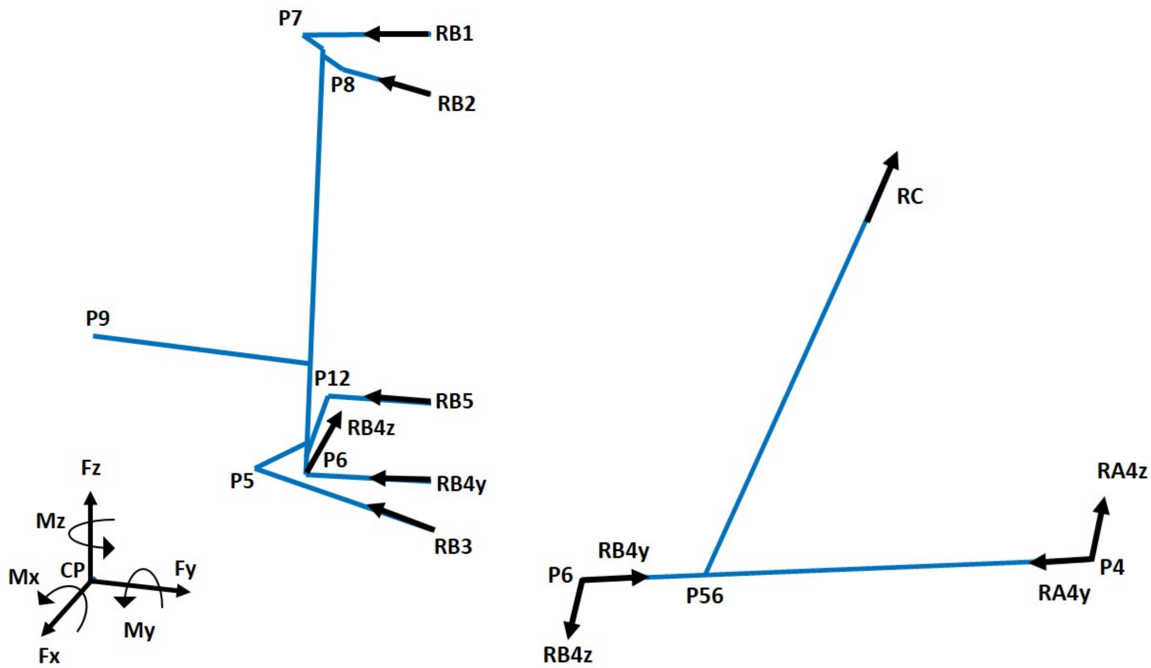

Figure 3.2: Free body diagram representing forces on knuckle, Lower control arm and spring

To determine the spring deflection due to the applied forces, equilibrium forces needs to be solved and the obtained reaction force in P56-55 spring needs to equated with $K_s.s$. Here, K_s is the spring stiffness and s is the spring deflection due to the applied force.

The equilibrium of the knuckle is solved first and later the equilibrium of the individual links are considered. The external forces are acting at the wheel in its contact point with the road. The forces generated on the 5 links are RB1, RB2, RB3, RB4y and RB4z respectively. RB1, RB2, RB3, RB4y and RB5 are the reaction forces from the subframe. Whereas, RB4z is the reaction force on the knuckle due to the spring force. For the given five link suspension, the wheel carrier equilibrium is calculated by the vectorial method mentioned below [1].

$$F_0 + RB1 \cdot \hat{d}_1 + RB2 \cdot \hat{d}_2 + RB3 \cdot \hat{d}_3 + RB4y \cdot \hat{d}_4 a + RB4z \cdot \hat{d}_4 b + RB5 \cdot \hat{d}_5 = 0 \quad (3.14)$$

Taking the moments about P6

$$M_0 + (\vec{b_{6,9}} \times F_0) + RB1 \cdot (\vec{b_{6,7}} \times \hat{d}_1) + RB2 \cdot (\vec{b_{6,8}} \times \hat{d}_2) + RB3 \cdot (\vec{b_{6,5}} \times \hat{d}_3) + RB5 \cdot (\vec{b_{6,12}} \times \hat{d}_5) = 0 \quad (3.15)$$

Where,
F_0 = Force vector
M_0 = Moment vector
$\hat{d_i}$ = unit vector between subframe and wheel-carrier hardpoints
$\vec{b_{ij}}$ = vector between wheel-carrier hardpoints

M_0 = External Moment + Moment at wheel center due to external forces at wheel contact point.
The total moment generated at the wheel center can be calculated as follows [3]:

$$M_0 = M + \vec{d_{9-CP}} \times F_0 \quad (3.16)$$

The direction vectors $\hat{d_i}$ and $\hat{b}_{ij}$ are used to resolve the forces in three (x,y,z) directions in 3D space which makes it easier to solve the equilibrium equations. The direction vectors can be calculated as follows .

$\hat{d}_3 = \frac{P5-P3}{d_{5-3}}$

$\hat{d}_3 = \frac{\hat{d}_{3x}}{d_{5-3}} + \frac{\hat{d}_{3y}}{d_{5-3}} + \frac{\hat{d}_{3z}}{d_{5-3}}$

$\vec{b_{65}} = P5 - P6$

The equations of equilibrium can be represented in form of a linear matrix as shown below. The forces and moments of the link are resolved along the three directions and are equated to the forces and moments at the wheel contact point [1].

$$\begin{bmatrix} \hat{d_{1x}} & \hat{d_{2x}} & \hat{d_{3x}} & \hat{d_{4ax}} & \hat{d_{5x}} & \hat{d_{4bx}} \\ \hat{d_{1y}} & \hat{d_{2y}} & \hat{d_{3y}} & \hat{d_{4ay}} & \hat{d_{5y}} & \hat{d_{4by}} \\ \hat{d_{1z}} & \hat{d_{2z}} & \hat{d_{3z}} & \hat{d_{4az}} & \hat{d_{5z}} & \hat{d_{4bz}} \\ (\vec{b_{6,7}} \times \hat{d}_1)_x & (\vec{b_{6,8}} \times \hat{d}_2)_x & (\vec{b_{6,5}} \times \hat{d}_5)_x & 0 & (\vec{b_{6,12}} \times \hat{d}_5)_x & 0 \\ (\vec{b_{6,7}} \times \hat{d}_1)_y & (\vec{b_{6,8}} \times \hat{d}_2)_y & (\vec{b_{6,5}} \times \hat{d}_5)_y & 0 & (\vec{b_{6,12}} \times \hat{d}_5)_y & 0 \\ (\vec{b_{6,7}} \times \hat{d}_1)_z & (\vec{b_{6,8}} \times \hat{d}_2)_z & (\vec{b_{6,5}} \times \hat{d}_5)_z & 0 & (\vec{b_{6,12}} \times \hat{d}_5)_z & 0 \end{bmatrix} \begin{bmatrix} RB1 \\ RB2 \\ RB3 \\ RB4y \\ RB5 \\ RB4z \end{bmatrix} = \begin{bmatrix} -F_x \\ -F_y \\ -F_z \\ -(M_x + \vec{b_{6,9}} F_x) \\ -(M_y + \vec{b_{6,9}} F_y) \\ -(M_z + \vec{b_{6,9}} F_z) \end{bmatrix} \quad (3.17)$$

The equilibrium equations of the Lower control arm are also expressed in form of a linear matrix as shown below. Few of the inputs to this matrix are obtained from solving eq 3.17.

$$\begin{bmatrix} -\hat{d_{4ay}} & -\hat{d_{4by}} & \hat{d_{4ay}} & \hat{d_{4by}} & \hat{d_{cy}} \\ -\hat{d_{4az}} & -\hat{d_{4bz}} & \hat{d_{4az}} & \hat{d_{4bz}} & \hat{d_{cz}} \\ (\vec{b_{6,4}} \times -\hat{d}_{4a})_z & (\vec{b_{6,4}} \times -\hat{d}_{4b})_z & 0 & 0 & (\vec{b_{56,4}} \times \hat{d}_c)_z \end{bmatrix} \begin{bmatrix} RB4y \\ RB4z \\ RA4y \\ RA4z \\ RC \end{bmatrix} = 0 \quad (3.18)$$

The obtained RC is then compared with the spring force $f(s) = RC - K_s.s$. If $f(s)$ is not equal to zero, then the solver changes the hardpoints and calculates the new unit vectors, computes the forces and evaluates $f(s)$ again. This is an iterative method and the solver iterates for different values of the parameters till the constraint function converges to zero. By this method, the solver tries to find the new position of static equilibrium.

3.4 Bushing Implementation

Bushings are the elastic elements made of rubber, polyurethane or similar materials. They are mounted on the suspension to absorb the impact force from the road bumps, reduce friction and to control the elasto-kinematic movements in the joints. Bushings play crucial role in achieving isolation for NVH and ride comfort. Bushings can be considered as a 3D spring with six degrees of freedom. Figure 3.3 represents three translations and three rotational stiffness defined to a bushing. The bushing are elastic elements and it results in compliance in the

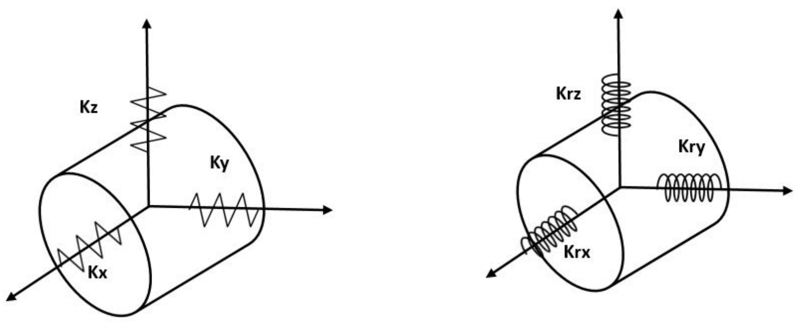

Figure 3.3: Translation and Rotation stiffness of the Bush

suspension system. The compliance needs to be well defined. For instance, generally the suspension system is stiff in the lateral direction, but is soft in the longitudinal direction for improving ride comfort. If the suspension is not stiff in the lateral direction, this can lead to undesired steering effects for the driver and can make it difficult for driving.

Due to external forces and the relative movement between the suspension links, the bushing deforms. These deformations can be considered in three primary directions of translation and rotation. s_x, s_y and s_z are the bushing translation deformations and s_{rx}, s_{ry}, s_{rz} are the bushing rotation deformations along x, y and z axes respectively. These deformations influence the position constraints and the equilibrium forces, which means that the equilibrium position will be slightly different than the purely kinematic mode. The stiffness matrix of a bushing is defined as [2],

$$K_T = \begin{bmatrix} K_x & 0 & 0 \\ 0 & K_y & 0 \\ 0 & 0 & K_z \end{bmatrix}, \qquad K_R = \begin{bmatrix} K_{rx} & 0 & 0 \\ 0 & K_{ry} & 0 \\ 0 & 0 & K_{rz} \end{bmatrix}$$

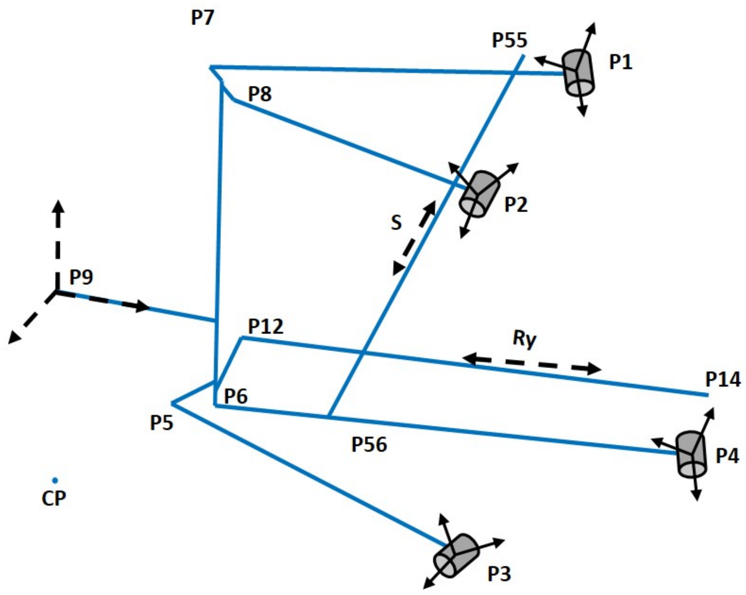

Figure 3.4: Four bushings implemented at LCA and UCA

Four Bushings are implemented at the subframe end of the lower and upper control arms as shown in figure 3.4. s_i is the deformation in the i^{th} bushing. At the equilibrium, the hardpoint position of the UCA mounts P1, P2 and LCA mounts P3, P4 changes due to the deformation s_i. The new positions of P1, P2, P3 and P4 are given by,

$$Pi_n = \begin{bmatrix} (Pi(x) - s_{ix}) \\ (Pi(y) - s_{iy}) \\ (Pi(z) - s_{iz}) \end{bmatrix}$$

As s_i is an unknown, the number of equations needs to be increased in order to solve the system. The position constraint equation for the P1-P7 link can be split into three equations as,

$$\begin{aligned}&(x_0 + R(1,1) \cdot P7_9(1) + R(1,2) \cdot P7_9(2) + R(1,3) \cdot P7_9(3)) \\ &- ((P_1(1) - s_{1x}) + R_1(1,1) \cdot P7_1(1) + R_1(1,2) \cdot P7_1(2) + R_1(1,3) \cdot P7_1(3)) = 0\end{aligned} \tag{3.19}$$

$$\begin{aligned}&(y_0 + R(2,1) \cdot P7_9(1) + R(2,2)7_9(2) + R(2,3)7_9(3)) \\ &- ((P_1(2) - s_{1y}) + R_1(2,1) \cdot P7_1(1) + R_1(2,2) \cdot P7_1(2) + R_1(2,3) \cdot P7_1(3)) = 0\end{aligned} \tag{3.20}$$

$$\begin{aligned}&(z_0 + R(3,1) \cdot P7_9(1) + R(3,2) \cdot P7_9(2) + R(3,3) \cdot P7_9(3)) \\ &- ((P_1(3) - s_{1z}) + R_1(3,1) \cdot P7_1(1) + R_1(3,2) \cdot P7_1(2) + R_1(3,3) \cdot P7_1(3)) = 0\end{aligned} \tag{3.21}$$

Here, the equation is formulated such that the coordinate P7 measured with respect to coordinate P9 and coordinate P1 should remain the same. Similar equations can be formulated for the links P2-P8, P3-P5 and P4-P6.

3.4.1 Bushing orientation

The bushing orientation needs to be included in the mathematical model to determine the bushing deformations in the local coordinate system. To capture this, two local coordinate systems were modelled at each bushing. One being fixed to the subframe and another being fixed to the lower control arm so the change in orientation can be captured with suspension movement.

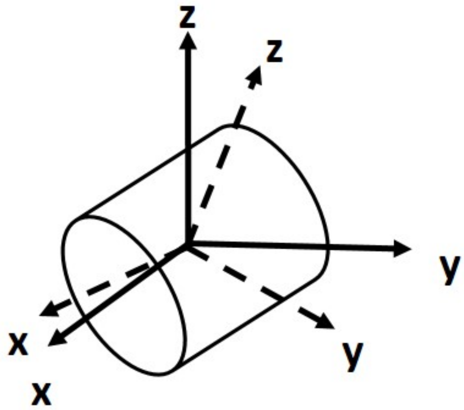

Figure 3.5: Bushing local coordinate systems

If ψ_I, θ_I, ϕ_I are the Euler angles of the initial bushing orientation which is fixed to the subframe and ψ_b, θ_b, ϕ_b are the Euler angles of the local coordinates of the bushing attached to the links, the rotation matrix is defined as follows [7]:

$$Rb_F = \begin{bmatrix} cos\psi_I \cdot cos\theta_I & cos\psi_I \cdot sin\theta_I . sin\phi_I - sin\psi_I \cdot cos\phi_I & cos\psi_I \cdot sin\theta_I \cdot cos\phi_I + sin\psi_I \cdot sin\phi_I \\ sin\psi_I \cdot cos\theta_I & sin\psi_I \cdot sin\theta_I \cdot sin\phi_I + cos\psi_I \cdot cos\phi_I & sin\psi_I \cdot sin\theta_I \cdot cos\phi_I - cos\psi_I \cdot sin\phi_I \\ -sin\theta_I & cos\theta_I \cdot sin\phi_I & cos\theta_I \cdot cos\phi_I \end{bmatrix}$$

The stiffness matrix can then be modified by multiplying it with the rotation matrix to orient the bushing with respect to the subframe.

$$K_T = Rb_F \times \begin{bmatrix} K_x & 0 & 0 \\ 0 & K_y & 0 \\ 0 & 0 & K_z \end{bmatrix}, \qquad K_R = Rb_F \times \begin{bmatrix} K_{rx} & 0 & 0 \\ 0 & K_{ry} & 0 \\ 0 & 0 & K_{rz} \end{bmatrix}$$

$$K_b = \begin{bmatrix} K_T & 0_{3\times3} \\ 0_{3\times3} & K_R \end{bmatrix}$$

This is the input to the mathematical model and the stiffness along x,y & z are defined about the bushing's local coordinate system. As the links move due to external forces, the bushing deforms. It becomes important to define one more rotation matrix of the bushing with respect to the links to constrain the rotational displacements of the bushings. For this, the Euler angles with respect to link are considered.

$$R_b = \begin{bmatrix} cos\psi_b \cdot cos\theta_b & cos\psi_b \cdot sin\theta_b \cdot sin\phi_b - sin\psi_b \cdot cos\phi_b & cos\psi_b \cdot sin\theta_b \cdot cos\phi_b + sin\psi_b \cdot sin\phi_b \\ sin\psi_b \cdot cos\theta_b & sin\psi_b \cdot sin\theta_b \cdot sin\phi_b + cos\psi_b \cdot cos\phi_b & sin\psi_b \cdot sin\theta_b \cdot cos\phi_b - cos\psi_b \cdot sin\phi_b \\ -sin\theta_b & cos\theta_b \cdot sin\phi_b & cos\theta_b \cdot cos\phi_b \end{bmatrix}$$

3.4.2 Including bushings in force constraints

In order to include elastic elements in the mathematical model, similar steps mentioned in section 3 can be adopted. On introducing a bushing in the system, the equilibrium equations of the knuckle and the link changes, but the forces can still be represented in form of a linear matrix with additional terms and equations.

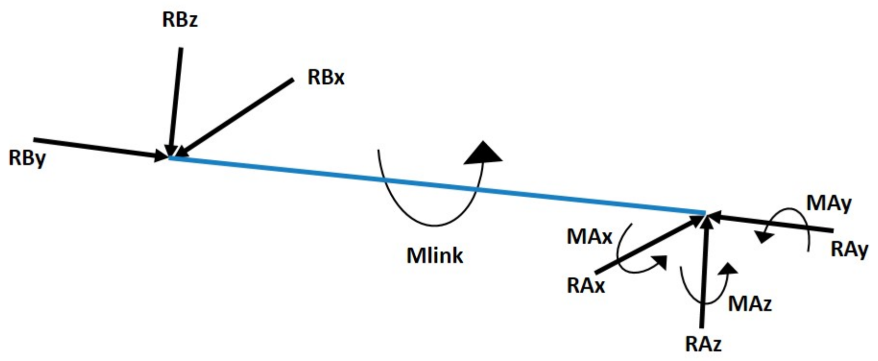

Figure 3.6: Bushing forces and moments on a link

When a bushing is introduced, forces in the link change as shown in the figure 3.6. The side of the link connected to the knuckle will have the forces RBx, RBy, RBz and the associated moments at the other end on the link. These will also result in addition of reaction forces RAx, RAy, RAz & bushing resistance moments MAx, MAy, MAz on the subframe side of the link. In order to capture the effect of the bushing, the moment along the link direction due to the bushing is also modelled.

These forces and moments can be added to the linear matrix corresponding to force and moment equations. The bushing deformations are constrained in different directions with force constraint equations. The resistance moment by the bushing is taken as a system input.

$$M = K_b \cdot (\theta - \theta_{init}) \tag{3.22}$$

where,
K_b = Bushing stiffness
θ = Bushing orientation (Changes as bushing deforms)
θ_{init} = Initial bushing orientation

Force equilibrium equations for link P1-P7:

$$-(RB7x \cdot \hat{d}_{7ax} + RB7y \cdot \hat{d}_{7bx} + RB7z \cdot \hat{d}_{7cx}) + RA1x \cdot \hat{d}_{1ax} + RA1y \cdot \hat{d}_{1bx} + RA1z \cdot \hat{d}_{1cx} = 0 \tag{3.23}$$

$$-(RB7x \cdot \hat{d}_{7ay} + RB7y \cdot \hat{d}_{7by} + RB7z \cdot \hat{d}_{7cy}) + RA1x \cdot \hat{d}_{1ay} + RA1y \cdot \hat{d}_{1by} + RA1z \cdot \hat{d}_{1cy} = 0 \tag{3.24}$$

$$-(RB7x \cdot \hat{d}_{7az} + RB7y \cdot \hat{d}_{7bz} + RB7z \cdot \hat{d}_{7cz}) + RA1x \cdot \hat{d}_{1az} + RA1y \cdot \hat{d}_{1bz} + RA1z \cdot \hat{d}_{1cz} = 0 \tag{3.25}$$

Moment equilibrium equations for link P1-P7 about P1:

$$RB7x \cdot (\vec{b_{1,7}} \times \hat{d}_{7a})_x + RB7y \cdot (\vec{b_{1,7}} \times \hat{d}_{7b})_x + RB7z \cdot (\vec{b_{1,7}} \times \hat{d}_{7c})_x + M_{link1} \cdot d_{1bx} - M_{1x} = 0 \tag{3.26}$$

$$RB7x \cdot (\vec{b_{1,7}} \times \hat{d}_{7a})_y + RB7y \cdot (\vec{b_{1,7}} \times \hat{d}_{7b})_y + RB7z \cdot (\vec{b_{1,7}} \times \hat{d}_{7c})_y + M_{link1} \cdot d_{1by} - M_{1y} = 0 \tag{3.27}$$

$$RB7x \cdot (\vec{b_{1,7}} \times \hat{d}_{7a})_z + RB7y \cdot (\vec{b_{1,7}} \times \hat{d}_{7b})_z + RB7z \cdot (\vec{b_{1,7}} \times \hat{d}_{7c})_z + M_{link1} \cdot d_{1bz} - M_{1z} = 0 \quad (3.28)$$

These equations are solved with kinematic force equations inside the nonlinear solver. The bushing reaction forces and the moments are calculated. The reaction forces are then constrained with the bushing stiffness. The force constraints can be of the form:

$$(RA1x \cdot \hat{d}_{1ax} + RA1y \cdot \hat{d}_{1bx} + RA1z \cdot \hat{d}_{1cx}) - K_{1x} \cdot s_{1x} = 0 \quad (3.29)$$

$$(RA1x \cdot \hat{d}_{1ay} + RA1y \cdot \hat{d}_{1by} + RA1z \cdot \hat{d}_{1cy}) - K_{1y} \cdot s_{1y} = 0 \quad (3.30)$$

$$(RA1x \cdot \hat{d}_{1az} + RA1y \cdot \hat{d}_{1bz} + RA1z \cdot \hat{d}_{1cz}) - K_{1z} \cdot s_{1z} = 0 \quad (3.31)$$

In the above equation, K_1 is the bushing stiffness and s_1 is the bushing deformation. All the forces in a particular direction at P1 is constrained using bushing stiffness values. Based on these values, the bushing deformations are obtained from the results of the non-linear solver. These force constraints can be added to represent the different bushing deformations.

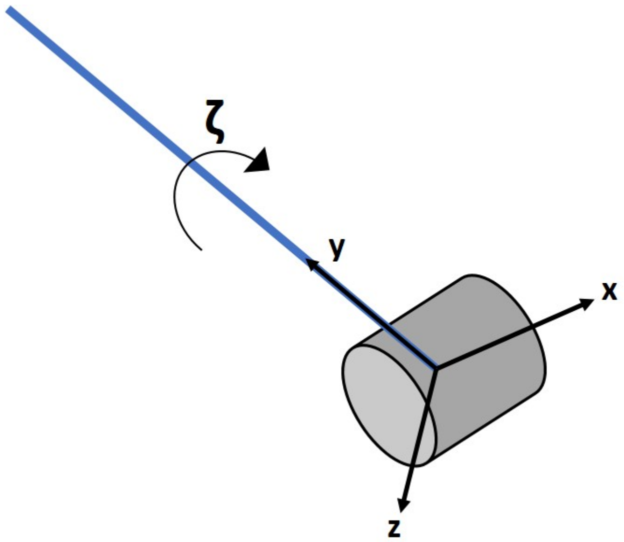

Figure 3.7: Rotation of link about the link direction

To constraint the rotational stiffness, one more rotation matrix is needed which is oriented along the link direction, M_{link}. The associated transformations are indicated below [12]:

$$R_L = \begin{bmatrix} cos\psi_L \cdot cos\theta_L & cos\psi_L \cdot sin\theta_L \cdot sin\phi_L - sin\psi_L \cdot cos\phi_L & cos\psi_L \cdot sin\theta_L \cdot cos\phi_L + sin\psi_L \cdot sin\phi_L \\ sin\psi_L \cdot cos\theta_L & sin\psi_L \cdot sin\theta_L \cdot sin\phi_L + cos\psi_L \cdot cos\phi_L & sin\psi_L \cdot sin\theta_L \cdot cos\phi_L - cos\psi_L \cdot sin\phi_L \\ -sin\theta_L & cos\theta_L \cdot sin\phi_L & cos\theta_L \cdot cos\phi_L \end{bmatrix}$$

$$A_{init} = R_L^{-1} \cdot Rb_F \quad (3.32)$$

$$\zeta_{init} = \tan^{-1}\left(\frac{A_{init}(1,3)}{A_{init}(1,1)}\right) \quad (3.33)$$

$$A = R_L^{-1} \cdot R_b \tag{3.34}$$

$$\zeta = \tan^{-1}\left(\frac{A(1,3)}{A(1,1)}\right) - \zeta_{init} \tag{3.35}$$

Where, ζ_{init} is the initial angle of rotation and ζ is the rotation of the link about its axis.

$$K_{rot} = R_L \cdot R \cdot K_R \tag{3.36}$$

$$M_{link} - \zeta \cdot K_{rot}(y) = 0 \tag{3.37}$$

Both the translation displacements and rotational displacements are now constrained. With the help of this methodology, it is possible to introduce 'n' number of bushings in the model. The bushings can be introduced in both the subframe or the knuckle side. The orientation of the bushings can also be adjusted based on the requirements.

Similarly, other links with bushings can also be solved for unknown reaction forces and its movement can be constrained using the bushing stiffness.

4 Modifications to the implemented methodology

The previously established methodology for five link suspension from chapter 3 can be implemented for other suspension systems as well. However, using the previously established methodology for modelling suspension systems like Four link or an Integral link suspension system can be quite complex.

When implementing the previous methodology, we first count the number of unknowns and equations for the system. In order to solve the set of unknowns, the system has to be completely constrained i.e, the number of unknown parameters and the equations should be equal.

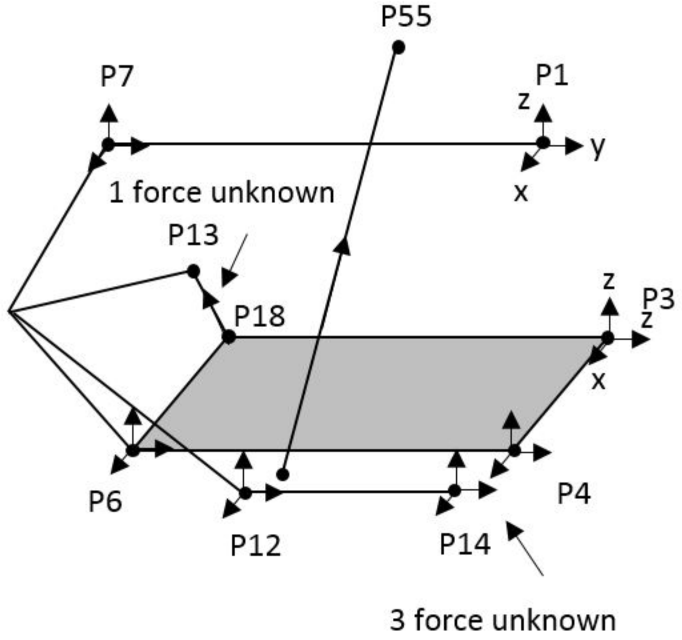

Figure 4.1: Number of force unknowns in an integral link suspension system

Consider the case of an integral link suspension system with bushings on the subframe for which we have the following unknown parameters when formulating the linear force matrix.

- We have 3 unknown forces at each joint in the system. Consider joints at Pt3, Pt4, Pt6, Pt7, Pt1, Pt12 and Pt14 leading to the number of unknowns being equal to 21.
- For joints at which the line of action of force is known, the number of unknown forces can be reduced to one. This holds good in the case of the integral link and the force for the spring system. This leads to another 2 unknowns.
- Since we have bushings at the end of the toe and camber link, we need to consider two more unknowns ζ (as mentioned in the previous section) in order to completely constrain the link rotation

Thus, we now have 26 unknowns in total and we need 26 equations to solve the system. We can formulate 24 equations from static equilibrium (3 moment and 3 force equations) for the 4 bodies knuckle, lower platform, toe and the camber link.

There is a deficit of 2 more equations and formulating it can be quite complex. The two equations need to be formulated such that the force matrix does not become singular and also the matrix is of full rank.

This problem can be overcome by using a different approach to formulate the equations for the non linear solver. In the previous methodology, the force constraints were solved in a linear force matrix and the non linear solver consisted of the position constraints and the equations to constrain the bushing translation movement, ζ rotation and spring displacement. In order to solve the above mismatch in the number of unknowns and equations, the non linear solver now is formulated such that it consists of both position constraints and force constraint equations.

The new methodology has the following main changes:

- Previously, the forces at which the bushings are present were taken as unknown forces. But these forces are now defined as system inputs to the force constraints.
- The parameters to the non linear solver are the unknown forces, translation and rotation of local coordinate systems. Thus the non linear solver, determines these values through iterative method.
- The need for a linear force matrix is eliminated. Thus the solver consists of both position and force constraints which makes it easier to match the number of unknown parameters and the equations

When we again consider integral link suspension system, with the help of the new method, the number of unknowns can now be calculated as follows:

- 24 unknowns from the introduction of 4 local coordinate systems for the 4 bodies namely knuckle, lower platform, toe and camber link
- Since bushing forces are defined as system inputs, the only force unknowns are at Pt7, Pt12, Pt18, Pt6 and the spring force. This adds another 11 unknowns to the system
- 3 more unknowns to determine the ζ rotation and spring displacement

Thus, we now have a system with 38 unknowns. In order to constrain the system, we can formulate 11 position constraint equations. Then we have 24 equations for static equilibrium of 4 bodies. Finally, 2 equations to constrain the ζ rotation and one equation to constrain the spring displacement. So we now have a system with 38 unknowns and 38 equations. This method completely eliminates the necessity to formulate extra equations and is less complex.

In the current thesis work, the new methodology is implemented for a Four link and an Integral link suspension system which will be explained in detail in the following sections.

5 Four Link Suspension

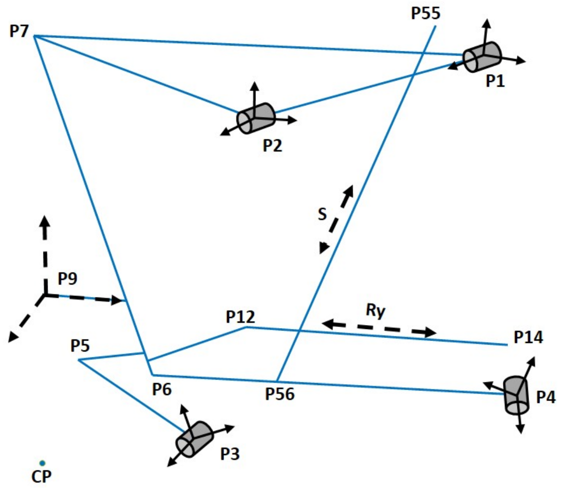

Figure 5.1: Four link suspension

The modelling of the four link suspension is very similar to that of a 5 link suspension. The single point links can be modelled using similar methodologies as explained in the previous sections. The main modelling challenge is the upper control arm. In the case of a four link suspension system, the number of force and position constraints unknowns sum up to be 29 in total. With the help of the new methodology it is easier to match the number of unknowns and equations.

5.1 Position Constraint Equations

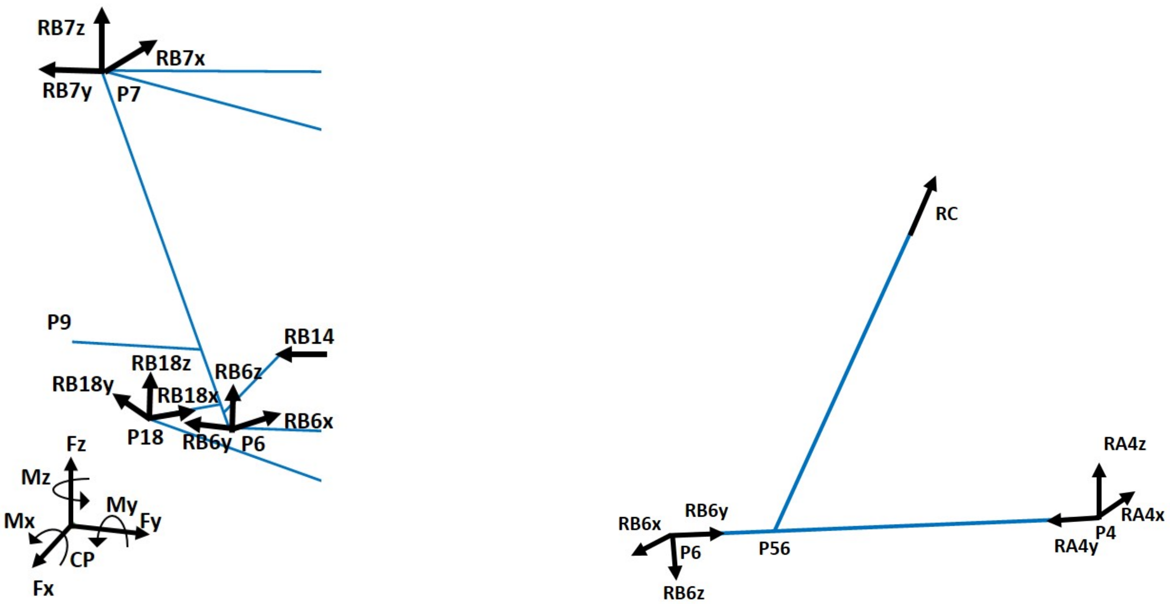

Figure 5.2: Free body diagram representing forces on knuckle, LCA and spring for a four link suspension

In order to formulate the position constraint equations, we need to introduce a few local coordinate systems. The local coordinates systems are introduced at point P9, P2, P4 and P3. With the help of these coordinates it is possible to trace the movement of different points in the system. For example, the local coordinates system at P2 is sufficient to define all the points on the upper control arm without the need of introducing additional unknown parameters.

Since there is a Bushing at P2, the position of P7 viewed from the P2 coordinate and the P9 coordinate is the same as it is a common point to both the upper control arm and the knuckle. The same can be represented as shown in the equations below.

$$\begin{aligned}&(x_0 + R(1,1) \cdot P7_9(1) + R(1,2) \cdot P7_9(2) + R(1,3) \cdot P7_9(3))\\&-((P_1(1) - s_{1x}) + R_1(1,1) \cdot P7_1(1) + R_1(1,2) \cdot P7_1(2) + R_1(1,3) \cdot P7_1(3)) = 0\end{aligned} \tag{5.1}$$

$$\begin{aligned}&(y_0 + R(2,1) \cdot P7_9(1) + R(2,2) \cdot P7_9(2) + R(2,3) \cdot P7_9(3))\\&-((P_1(2) - s_{1y}) + R_1(2,1) \cdot P7_1(1) + R_1(2,2) \cdot P7_1(2) + R_1(2,3) \cdot P7_1(3)) = 0\end{aligned} \tag{5.2}$$

$$\begin{aligned}&(z_0 + R(3,1) \cdot P7_9(1) + R(3,2) \cdot P7_9(2) + R(3,3) \cdot P7_9(3))\\&-((P_1(3) - s_{1z}) + R_1(3,1) \cdot P7_1(1) + R_1(3,2) \cdot P7_1(2) + R_1(3,3) \cdot P7_1(3)) = 0\end{aligned} \tag{5.3}$$

$$\begin{aligned}&(x_0 + R(1,1) \cdot P12_9(1) + R(1,2) \cdot P12_9(2) + R(1,3) \cdot P12_9(3) - P14(1))^2 +\\&(y_0 + R(2,1) \cdot P12_9(1) + R(2,2) \cdot P12_9(2) + R(2,3) \cdot P12_9(3) - (P14(2) - Ry))^2 +\\&(z_0 + R(3,1) \cdot P12_9(1) + R(3,2) \cdot P12_9(2) + R(3,3) \cdot P12_9(3) - P14(3))^2 - d_{12-14}^2 = 0\end{aligned} \tag{5.4}$$

P6 is also a common point between the knuckle and the lower control arm. Thus the position of P6 viewed from the knuckle local coordinate and the coordinate at P4 remains the same.

$$\begin{aligned}&(x_0 + R(1,1) \cdot P6_9(1) + R(1,2) \cdot P6_9(2) + R(1,3) \cdot P6_9(3))\\&-((P4(1) - s_{4x}) + R_4(1,1) \cdot P6_4(1) + R_4(1,2) \cdot P6_4(2) + R_4(1,3) \cdot P6_4(3)) = 0\end{aligned} \tag{5.5}$$

$$\begin{aligned}&(y_0 + R(2,1) \cdot P6_9(1) + R(2,2) \cdot P6_9(2) + R(2,3) \cdot P6_9(3))\\&-((P4(2) - s_{4y}) + R_4(2,1) \cdot P6_4(1) + R_4(2,2) \cdot P6_4(2) + R_4(2,3) \cdot P6_4(3)) = 0\end{aligned} \tag{5.6}$$

$$\begin{aligned}&(z_0 + R(3,1) \cdot P6_9(1) + R(3,2) \cdot P6_9(2) + R(3,3) \cdot P6_9(3))\\&-((P4(3) - s_{4z}) + R_4(3,1) \cdot P6_4(1) + R_4(3,2) \cdot P6_4(2) + R_4(3,3) \cdot P6_4(3)) = 0\end{aligned} \tag{5.7}$$

$$\begin{aligned}&((P4(1) - s_{4x}) + R_4(1,1) \cdot P56_4(1) + R_4(1,2) \cdot P56_4(2) + R_4(1,3) \cdot P56_4(3)\\&- P55(1))^2 + ((P4(2) - s_{4y}) + R_4(2,1) \cdot P56_4(1) + R_4(2,2) \cdot P56_4(2)\\&+ R_4(2,3) \cdot P56_4(3) - P55(2))^2 + ((P4(3) - s_{4z}) + R_4(3,1) \cdot P56_4(1)\\&+ R_4(3,2) \cdot P56_4(2) + R_4(3,3) \cdot P56_4(3) - P55(3))^2 - (d_{56-55} - s)^2 = 0\end{aligned} \tag{5.8}$$

A distance constraint equation is split into three equations. This method is used when modelling links with bushing. P18 is a common point on the knuckle and the link, thus its position when viewed from two different coordinates (one at P9 and one at P3) remains the same.

$$\begin{aligned}&(x_0 + R(1,1) \cdot P18_9(1) + R(1,2) \cdot P18_9(2) + R(1,3) \cdot P18_9(3)) \\ &- ((P_3(1) - s_{3x}) + R_3(1,1) \cdot P18_3(1) + R_3(1,2) \cdot P18_3(2) + R_3(1,3) \cdot P18_3(3)) = 0\end{aligned} \tag{5.9}$$

$$\begin{aligned}&(y_0 + R(2,1) \cdot P18_9(1) + R(2,2) \cdot P18_9(2) + R(2,3) \cdot P18_9(3)) \\ &- ((P_3(2) - s_{3y}) + R_3(2,1) \cdot P18_3(1) + R_3(2,2) \cdot P18_3(2) + R_3(2,3) \cdot P18_3(3)) = 0\end{aligned} \tag{5.10}$$

$$\begin{aligned}&(z_0 + R(3,1) \cdot P18_9(1) + R(3,2) \cdot P18_9(2) + R(3,3) \cdot P18_9(3)) \\ &- ((P_3(3) - s_{3z}) + R_3(3,1) \cdot P18_3(1) + R_3(3,2) \cdot P18_3(2) + R_3(3,3) \cdot P18_3(3)) = 0\end{aligned} \tag{5.11}$$

5.2 Force Constraints

The static equilibrium equations of 4 bodies are considered to formulate the forces constraints. The bushing forces at P3, P1, P2, P4 are given as inputs to the system and the reaction forces at the knuckle are considered as unknowns forces. The non linear solver solves the system of position and force constraint equations and yields the values of the reaction forces as output.

Force equilibrium equations for the Knuckle:

$$\begin{aligned}&Fx + RB6x \cdot \hat{d}_{6ax} + RB6y \cdot \hat{d}_{6bx} + RB6z \cdot \hat{d}_{6cx} + RB7x \cdot \hat{d}_{7ax} + RB7y \cdot \hat{d}_{7bx} \\ &+ RB7z \cdot \hat{d}_{7cx} + RB14 \cdot \hat{d}_{14x} + RB18x \cdot \hat{d}_{18ax} + RB18y \cdot \hat{d}_{18bx} + RB18z \cdot \hat{d}_{18cx} = 0\end{aligned} \tag{5.12}$$

$$\begin{aligned}&Fy + RB6x \cdot \hat{d}_{6ay} + RB6y \cdot \hat{d}_{6by} + RB6z \cdot \hat{d}_{6cy} + RB7x \cdot \hat{d}_{7ay} + RB7y \cdot \hat{d}_{7by} \\ &+ RB7z \cdot \hat{d}_{7cy} + RB14 \cdot \hat{d}_{14y} + RB18y \cdot \hat{d}_{18ay} + RB18y \cdot \hat{d}_{18by} + RB18z \cdot \hat{d}_{18cy} = 0\end{aligned} \tag{5.13}$$

$$\begin{aligned}&Fz + RB6x \cdot \hat{d}_{6az} + RB6y \cdot \hat{d}_{6bz} + RB6z \cdot \hat{d}_{6cz} + RB7x \cdot \hat{d}_{7az} + RB7y \cdot \hat{d}_{7bz} \\ &+ RB7z \cdot \hat{d}_{7cz} + RB14 \cdot \hat{d}_{14z} + RB18z \cdot \hat{d}_{18az} + RB18y \cdot \hat{d}_{18bz} + RB18z \cdot \hat{d}_{18cz} = 0\end{aligned} \tag{5.14}$$

Moment equilibrium equations for the Knuckle about P6:

$$\begin{aligned}&(M_x + \vec{b_{6,9}} F_x) + RB14 \cdot (\vec{b_{6,12}} \times \hat{d}_{14})_x + RB18x \cdot (\vec{b_{6,18}} \times \hat{d}_{18a})_x \\ &+ RB18y \cdot (\vec{b_{6,18}} \times \hat{d}_{18b})_x + RB18z \cdot (\vec{b_{6,18}} \times \hat{d}_{18c})_x + RB7x \\ &\cdot (\vec{b_{6,7}} \times \hat{d}_{7a})_x + RB7y.(\vec{b_{6,7}} \times \hat{d}_{7b})_x + RB7z \cdot (\vec{b_{6,7}} \times \hat{d}_{7c})_x = 0\end{aligned} \tag{5.15}$$

$$\begin{aligned}&(M_y + \vec{b_{6,9}} F_y) + RB14 \cdot (\vec{b_{6,12}} \times \hat{d}_{14})_y + RB18x \cdot (\vec{b_{6,18}} \times \hat{d}_{18a})_y \\ &+ RB18y \cdot (\vec{b_{6,18}} \times \hat{d}_{18b})_y + RB18z \cdot (\vec{b_{6,18}} \times \hat{d}_{18c})_y + RB7x \\ &\cdot (\vec{b_{6,7}} \times \hat{d}_{7a})_y + RB7y \cdot (\vec{b_{6,7}} \times \hat{d}_{7b})_y + RB7z \cdot (\vec{b_{6,7}} \times \hat{d}_{7c})_y = 0\end{aligned} \tag{5.16}$$

$$\begin{aligned}&(M_z + \vec{b_{6,9}} F_z) + RB14 \cdot (\vec{b_{6,12}} \times \hat{d}_{14})_z + RB18x \cdot (\vec{b_{6,18}} \times \hat{d}_{18a})_z \\ &+ RB18y \cdot (\vec{b_{6,18}} \times \hat{d}_{18b})_z + RB18z \cdot (\vec{b_{6,18}} \times \hat{d}_{18c})_z + RB7x \\ &\cdot (\vec{b_{6,7}} \times \hat{d}_{7a})_z + RB7y \cdot (\vec{b_{6,7}} \times \hat{d}_{7b})_z + RB7z \cdot (\vec{b_{6,7}} \times \hat{d}_{7c})_z = 0\end{aligned} \tag{5.17}$$

Force equilibrium equations for Upper control arm:

$$-(RB7x \cdot \hat{d}_{7ax} + RB7y \cdot \hat{d}_{7bx} + RB7z \cdot \hat{d}_{7cx}) + K_{1x} \cdot s_{1x} + K_{2x} \cdot s_{2x} = 0 \tag{5.18}$$

$$-(RB7x \cdot \hat{d}_{7ay} + RB7y \cdot \hat{d}_{7by} + RB7z \cdot \hat{d}_{7cy}) + K_{1y} \cdot s_{1y} + K_{2y} \cdot s_{2y} = 0 \tag{5.19}$$

$$-(RB7x \cdot \hat{d}_{7az} + RB7y \cdot \hat{d}_{7bz} + RB7z \cdot \hat{d}_{7cz}) + K_{1z} \cdot s_{1z} + K_{2z} \cdot s_{2z} = 0 \tag{5.20}$$

Moment equilibrium equations for Upper control arm about P1:

$$\begin{aligned}&RB7x \cdot (\vec{b_{1,7}} \times \hat{d}_{7a})_x + RB7y \cdot (\vec{b_{1,7}} \times \hat{d}_{7b})_x + RB7z \cdot (\vec{b_{1,7}} \times \hat{d}_{7c})_x + K_{2x} \\ &\cdot (\vec{b_{1,2}} \times \hat{d}_{2a})_x + K_{2y} \cdot (\vec{b_{1,2}} \times \hat{d}_{2b})_x + K_{2z} \cdot (\vec{b_{1,2}} \times \hat{d}_{2c})_x - M_{1x} - M_{2x} = 0\end{aligned} \tag{5.21}$$

$$\begin{aligned}&RB7x.(\vec{b_{1,7}} \times \hat{d}_{7a})_y + RB7y \cdot (\vec{b_{1,7}} \times \hat{d}_{7b})_y + RB7z \cdot (\vec{b_{1,7}} \times \hat{d}_{7c})_y + K_{2x} \\ &\cdot (\vec{b_{1,2}} \times \hat{d}_{2a})_y + K_{2y} \cdot (\vec{b_{1,2}} \times \hat{d}_{2b})_y + K_{2z} \cdot (\vec{b_{1,2}} \times \hat{d}_{2c})_y - M_{1y} - M_{2y} = 0\end{aligned} \tag{5.22}$$

$$\begin{aligned}&RB7x \cdot (\vec{b_{1,7}} \times \hat{d}_{7a})_z + RB7y \cdot (\vec{b_{1,7}} \times \hat{d}_{7b})_z + RB7z \cdot (\vec{b_{1,7}} \times \hat{d}_{7c})_z + K_{2x} \\ &\cdot (\vec{b_{1,2}} \times \hat{d}_{2a})_z + K_{2y} \cdot (\vec{b_{1,2}} \times \hat{d}_{2b})_z + K_{2z} \cdot (\vec{b_{1,2}} \times \hat{d}_{2c})_z - M_{1z} - M_{2z} = 0\end{aligned} \tag{5.23}$$

Force equilibrium equations for Lower control arm:

$$-(RB6x \cdot \hat{d}_{6ax} + RB6y \cdot \hat{d}_{6bx} + RB6z \cdot \hat{d}_{6cx}) + K_{4x} \cdot s_{4x} + RC1 \cdot \hat{d}_{56-55x} = 0 \tag{5.24}$$

$$-(RB6x \cdot \hat{d}_{6ay} + RB6y \cdot \hat{d}_{6by} + RB6z \cdot \hat{d}_{6cy}) + K_{4y} \cdot s_{4y} + RC1 \cdot \hat{d}_{56-55y} = 0 \tag{5.25}$$

$$-(RB6x \cdot \hat{d}_{6az} + RB6y \cdot \hat{d}_{6bz} + RB6z \cdot \hat{d}_{6cz}) + K_{4z} \cdot s_{4z} + RC1 \cdot \hat{d}_{56-55z} = 0 \tag{5.26}$$

Moment equilibrium equations for Lower control arm about P4:

$$\begin{aligned}&RB6x \cdot (\vec{b_{4,6}} \times \hat{d}_{6a})_x + RB6y \cdot (\vec{b_{4,6}} \times \hat{d}_{6b})_x + RB6z \\ &\cdot (\vec{b_{4,6}} \times \hat{d}_{6c})_x + RC1 \cdot (\vec{b_{4,56}} \times \hat{d}_{56})_x - M_{4x} + M_4 \cdot d_{4ay} = 0\end{aligned} \tag{5.27}$$

$$\begin{aligned}&RB6x \cdot (\vec{b_{4,6}} \times \hat{d}_{6a})_y + RB6y \cdot (\vec{b_{4,6}} \times \hat{d}_{6b})_y + RB6z \\ &\cdot (\vec{b_{4,6}} \times \hat{d}_{6c})_y + RC1 \cdot (\vec{b_{4,56}} \times \hat{d}_{56})_y - M_{4y} + M_4 \cdot d_{4by} = 0\end{aligned} \tag{5.28}$$

$$\begin{aligned}&RB6x \cdot (\vec{b_{4,6}} \times \hat{d}_{6a})_z + RB6y \cdot (\vec{b_{4,6}} \times \hat{d}_{6b})_z + RB6z \\ &\cdot (\vec{b_{4,6}} \times \hat{d}_{6c})_z + RC1 \cdot (\vec{b_{4,56}} \times \hat{d}_{56})_z - M_{4z} + M_4 \cdot d_{4cz} = 0\end{aligned} \tag{5.29}$$

Equation to constrain the zeta rotation along the lower control arm:

$$M_4 - \zeta_4 \cdot K_{rot4}(y) = 0 \tag{5.30}$$

Force equilibrium equations for the link P3-P18:

$$-(RB18x \cdot \hat{d}_{18ax} + RB18y \cdot \hat{d}_{18bx} + RB18z \cdot \hat{d}_{18cx}) + K_{3x} \cdot s_{3x} = 0 \tag{5.31}$$

$$-(RB18x \cdot \hat{d}_{18ay} + RB18y \cdot \hat{d}_{18by} + RB18z \cdot \hat{d}_{18cy}) + K_{3y} \cdot s_{3y} = 0 \tag{5.32}$$

$$-(RB18x \cdot \hat{d}_{18az} + RB18y \cdot \hat{d}_{18bz} + RB18z \cdot \hat{d}_{18cz}) + K_{3z} \cdot s_{3z} = 0 \tag{5.33}$$

Moment equilibrium equations for the link P3-P18 about P3:

$$RB18x \cdot (\vec{b_{3,18}} \times \hat{d}_{18a})_x + RB18y \cdot (\vec{b_{3,18}} \times \hat{d}_{18b})_x + RB18z \cdot (\vec{b_{3,18}} \times \hat{d}_{18c})_x - M_{3x} + M_3 \cdot d_{3ay} = 0 \tag{5.34}$$

$$RB18x \cdot (\vec{b_{3,18}} \times \hat{d}_{18a})_y + RB18y \cdot (\vec{b_{3,18}} \times \hat{d}_{18b})_y + RB18z \cdot (\vec{b_{3,18}} \times \hat{d}_{18c})_y - M_{3y} + M_3 \cdot d_{3by} = 0 \tag{5.35}$$

$$RB18x \cdot (\vec{b_{3,18}} \times \hat{d}_{18a})_z + RB18y \cdot (\vec{b_{3,18}} \times \hat{d}_{18b})_z + RB18z \cdot (\vec{b_{3,18}} \times \hat{d}_{18c})_z - M_{3z} + M_3 \cdot d_{3cy} = 0 \tag{5.36}$$

Equation to constrain the zeta rotation along the link P3-P18:

$$M_3 - \zeta_3 \cdot K_{rot3}(y) = 0 \tag{5.37}$$

Equation to constrain the spring displacement:

$$Rc - K_s \cdot s = 0 \tag{5.38}$$

6 Integral Link Suspension

After the analysis of the four link suspension, the methodology is tested for a complicated suspension system such as Integral link suspension. In the four link suspension system the upper control arm is a triangular shaped element with two joints on subframe and single point joint on knuckle. Whereas, in integral link, the lower control platform is a trapezoidal structure with two joints on the subframe, one at the knuckle and one at the integral link.

Four local coordinate systems are introduced at P9, P1, P4 and P14. x_0, y_0, z_0 denote the wheel center coordinates. The total number of unknowns defined in the position constraint model are, [x_0, y_0, z_0, ϕ, θ, ψ], [ϕ_4, θ_4, ψ_4], [ϕ_1, θ_1, ψ_1], [ϕ_{14}, θ_{14}, ψ_{14}], and s. So, total 16 unknowns are there in the position constraint modelling.

The following image shows the free body diagram of the integral link suspension. The equilibrium equations are considered for four bodies namely knuckle, lower control platform, toe link and camber link.

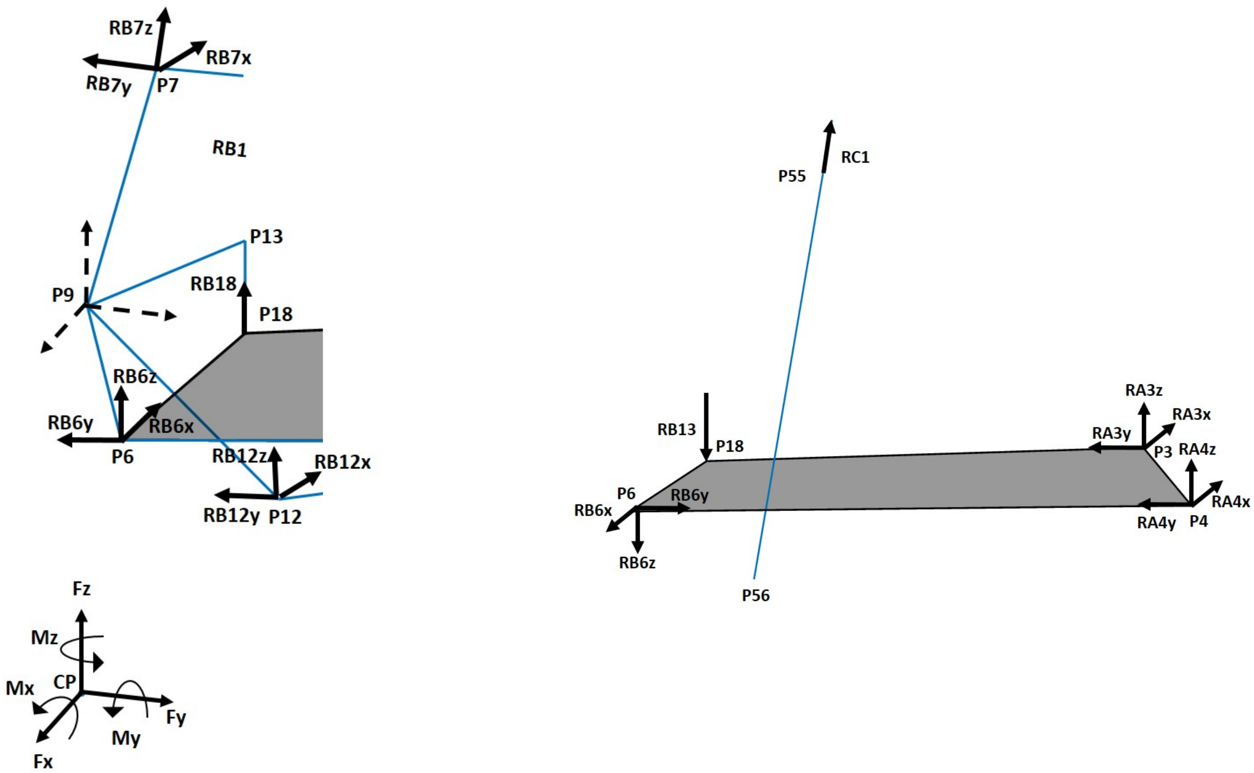

Figure 6.1: Free body diagram representing forces on knuckle, LCA and spring for an integral link suspension

In integral link suspension, bushings at P1 and P14 can be modelled using the same methodology discussed in the five link suspension. However, bushings at P3 and P4 needs to be modelled using the methodology discussed in the four link suspension as they both share a common body.

When the bushings are added at the subframe ends, the forces at P7, P1, P12 and P14 needs to be split into three forces in x, y and z directions. Which means existing RB1 force is replaced with [RB7x, RB7y, RB7z] at P7 and [RA1x, RA1y, RA1z] at P1. Similarly, RB14 can be replaced with [RB12x RB12y RB12z] at P12 and [RA14x RA14y RA14z] at P14.

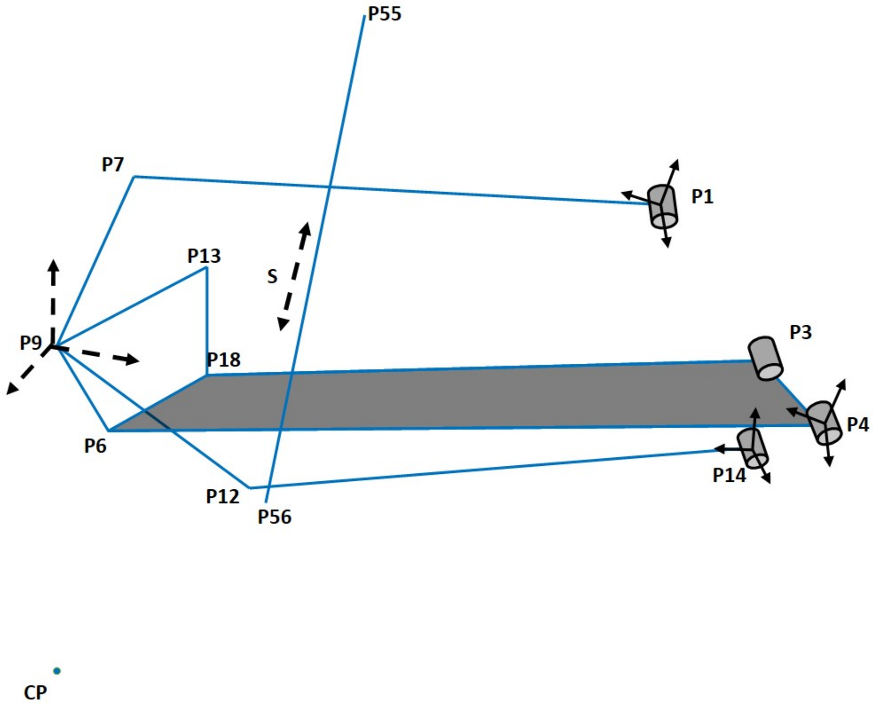

Figure 6.2: Integral link suspension with bushings at subframe end

The unknown forces are identified as [RB7x, RB7y, RB7z], [RB6x, RB6y, RB6z], [RB12x, RB12y, RB12z], [RA1x, RA1y, RA1z], [RA14x, RA14y, RA14z], [RA3x, RA3y, RA3z], [RA4x, RA4y, RA4z], RB13, RC, M1, M2 contributing to a total of 25 reaction forces. However, reaction forces at the subframe end can be expressed as K.s (bushing stiffness × bushing deformation).

$$\begin{bmatrix} RAix \\ RAiy \\ RAiz \end{bmatrix} = \begin{bmatrix} K_{ix} \cdot s_{ix} \\ K_{iy} \cdot s_{iy} \\ K_{iz} \cdot s_{iz} \end{bmatrix}$$

As, the hardpoint P3 can be measured with respect to the local coordinate at P4, the bushing deformations at P3 i.e $[s_{3x} \ s_{3y} \ s_{3z}]$ can no longer be treated as an unknown. This reduces the number of unknown reaction forces to 22. There are 16 unknowns in position constraint modelling and 22 in force constraint modelling. Total of 38 unknowns needs to be solved with 38 equations.

The position of P7 viewed from coordinate at P9 and coordinate at P1 remains the same. This is modelled as 3 equations as shown below.

$$\begin{aligned} &(x_0 + R(1,1) \cdot P7_9(1) + R(1,2) \cdot P7_9(2) + R(1,3) \cdot P7_9(3) \\ &- ((P1(1) - s_{1x}) + R_1(1,1) \cdot P7_1(1) + R_1(1,2) \cdot P7_1(2) + R_1(1,3) \cdot P7_1(3))) = 0 \end{aligned} \tag{6.1}$$

$$(y_0 + R(2,1) \cdot P7_9(1) + R(2,2) \cdot P7_9(2) + R(2,3) \cdot P7_9(3) \\ - ((P1(2) - s_{1y}) + R_1(2,1) \cdot P7_1(1) + R_1(2,2) \cdot P7_1(2) + R_1(2,3) \cdot P7_1(3))) = 0 \tag{6.2}$$

$$(z_0 + R(3,1) \cdot P7_9(1) + R(3,2) \cdot P7_9(2) + R(3,3) \cdot P7_9(3) \\ - ((P1(3) - s_{1z}) + R_1(3,1) \cdot P7_1(1) + R_1(3,2) \cdot P7_1(2) + R_1(3,3) \cdot P7_1(3))) = 0 \tag{6.3}$$

A local coordinate is introduced at P14 due to the introduction of a bushing at that point. So the position of P12 when viewed from the coordinate at P9 is same as that when viewed from the coordinate at P14.

$$(x_0 + R(1,1) \cdot P12_9(1) + R(1,2) \cdot P12_9(2) + R(1,3) \cdot P12_9(3) - ((P14(1) - s_{14x}) \\ + R_{14}(1,1) \cdot P12_{14}(1) + R_{14}(1,2) \cdot P12_{14}(2) + R_{14}(1,3) \cdot P12_{14}(3))) = 0 \tag{6.4}$$

$$(y_0 + R(2,1) \cdot P12_9(1) + R(2,2) \cdot P12_9(2) + R(2,3) \cdot P12_9(3) - ((P14(2) - s_{14y}) \\ + R_{14}(2,1) \cdot P12_{14}(1) + R_{14}(2,2) \cdot P12_{14}(2) + R_{14}(2,3) \cdot P12_{14}(3))) = 0 \tag{6.5}$$

$$(z_0 + R(3,1) \cdot P12_9(1) + R(3,2) \cdot P12_9(2) + R(3,3) \cdot P12_9(3) - ((P14(3) - s_{14z}) \\ + R_{14}(3,1) \cdot P12_{14}(1) + R_{14}(3,2) \cdot P12_{14}(2) + R_{14}(3,3) \cdot P12_{14}(3))) = 0 \tag{6.6}$$

The point P13 lies on the knuckle and is referenced with the coordinate at P9. The point P18 lies on the lower platform and is referenced with the coordinate at P4. With the help of this reference, the distance constraint between the point P13 and P18 is formulated as shown below.

$$\begin{aligned} &((x_0 + R(1,1) \cdot P13_9(1) + R(1,2) \cdot P13_9(2) + R(1,3) \cdot P13_9(3)) - \\ &((P4(1) - s_{4x}) + R_4(1,1) \cdot P18_4(1) + R_4(1,2) \cdot P18_4(2) + R_4(1,3) \cdot P18_4(3)))^2 + \\ &((y_0 + R(2,1) \cdot P13_9(1) + R(2,2) \cdot P13_9(2) + R(2,3) \cdot P13_9(3)) - \\ &((P4(2) - s_{4y}) + R_4(2,1) \cdot P18_4(1) + R_4(2,2) \cdot P18_4(2) + R_4(2,3) \cdot P18_4(3)))^2 + \\ &((z_0 + R(3,1) \cdot P13_9(1) + R(3,2) \cdot P13_9(2) + R(3,3) \cdot P13_9(3)) - \\ &((P4(3) - s_{4z}) + R_4(3,1) \cdot P18_4(1) + R_4(3,2) \cdot P18_4(2) + R_4(3,3) \cdot P18_4(3)))^2 \\ &- d_{13-18}^2 = 0 \end{aligned} \tag{6.7}$$

P6 is a common point for the knuckle and the lower control arm, thus its position when viewed from the coordinate at P4 and P9 remains the same.

$$(x_0 + R(1,1) \cdot P6_9(1) + R(1,2) \cdot P6_9(2) + R(1,3) \cdot P6_9(3) \\ - ((P4(1) - s_{4x}) + R_4(1,1) \cdot P6_4(1) + R_4(1,2) \cdot P6_4(2) + R_4(1,3) \cdot P6_4(3))) = 0 \tag{6.8}$$

$$(y_0 + R(2,1) \cdot P6_9(1) + R(2,2) \cdot P6_9(2) + R(2,3) \cdot P6_9(3) \\ - ((P4(2) - s_{4y}) + R_4(2,1) \cdot P6_4(1) + R_4(2,2) \cdot P6_4(2) + R_4(2,3) \cdot P6_4(3))) = 0 \tag{6.9}$$

$$(z_0 + R(3,1) \cdot P6_9(1) + R(3,2) \cdot P6_9(2) + R(3,3) \cdot P6_9(3) \\ - ((P4(3) - s_{4z}) + R_4(3,1) \cdot P6_4(1) + R_4(3,2) \cdot P6_4(2) + R_4(3,3) \cdot P6_4(3))) = 0 \tag{6.10}$$

Point P56 is referenced with respect to the coordinate at P4 when defining the distance constraint between P55 and P56.

$$
\begin{aligned}
&((P4(1) - s_{4x}) + R_4(1,1) \cdot P56_4(1) + R_4(1,2) \cdot P56_4(2) + R_4(1,3) \cdot P56_4(3) \\
&- P55(1))^2 + ((P4(2) - s_{4y}) + R_4(2,1) \cdot P56_4(1) + R_4(2,2) \cdot P56_4(2) \\
&+ R_4(2,3) \cdot P56_4(3) - P55(2))^2 + ((P4(3) - s_{4z}) + R_4(3,1) \cdot P56_4(1) \\
&+ R_4(3,2) \cdot P56_4(2) + R_4(3,3) \cdot P56_4(3) - P55(3))^2 - (d_{56-55} - s)^2 = 0
\end{aligned} \tag{6.11}
$$

6.1 Force constrains for Integral link

The main modeling challenge in the case of the integral link is the lower platform. The number of unknowns on this platform can be reduced from 10 to 4 by using the bushing forces as the inputs. Since P3 and P4 lie on the same body it is considered that both points have same orientation during suspension movement. Static equilibrium equations for 4 bodies are considered here.

Force equilibrium equations for the Knuckle:

$$
\begin{aligned}
&Fx + RB6x \cdot \hat{d}_{6ax} + RB6y \cdot \hat{d}_{6bx} + RB6z \cdot \hat{d}_{6cx} + RB7x \cdot \hat{d}_{7ax} + RB7y \cdot \hat{d}_{7bx} \\
&+ RB7z \cdot \hat{d}_{7cx} + RB12x \cdot \hat{d}_{12ax} + RB12y \cdot \hat{d}_{12bx} + RB12z \cdot \hat{d}_{12cx} + RB13 \cdot \hat{d}_{13x} = 0
\end{aligned} \tag{6.12}
$$

$$
\begin{aligned}
&Fy + RB6x \cdot \hat{d}_{6ay} + RB6y \cdot \hat{d}_{6by} + RB6z \cdot \hat{d}_{6cy} + RB7x \cdot \hat{d}_{7ay} + RB7y \cdot \hat{d}_{7by} \\
&+ RB7z \cdot \hat{d}_{7cy} + RB12x \cdot \hat{d}_{12ay} + RB12y \cdot \hat{d}_{12by} + RB12z \cdot \hat{d}_{12cy} + RB13 \cdot \hat{d}_{13y} = 0
\end{aligned} \tag{6.13}
$$

$$
\begin{aligned}
&Fz + RB6x \cdot \hat{d}_{6az} + RB6y \cdot \hat{d}_{6bz} + RB6z \cdot \hat{d}_{6cz} + RB7x \cdot \hat{d}_{7az} + RB7y \cdot \hat{d}_{7bz} \\
&+ RB7z \cdot \hat{d}_{7cz} + RB12x \cdot \hat{d}_{12az} + RB12y \cdot \hat{d}_{12bz} + RB12z \cdot \hat{d}_{12cz} + RB13 \cdot \hat{d}_{13z} = 0
\end{aligned} \tag{6.14}
$$

Moment equilibrium equations for the Knuckle about P6:

$$
\begin{aligned}
&(M_x + \vec{b_{6,9}} F_x) + RB7x \cdot (\vec{b_{6,7}} \times \hat{d}_{7a})_x + RB7y \cdot (\vec{b_{6,7}} \times \hat{d}_{7b})_x \\
&+ RB7z \cdot (\vec{b_{6,7}} \times \hat{d}_{7c})_x + RB12x \cdot (\vec{b_{6,12}} \times \hat{d}_{12a})_x + RB12y \\
&\cdot (\vec{b_{6,12}} \times \hat{d}_{12b})_x + RB12z \cdot (\vec{b_{6,12}} \times \hat{d}_{12c})_x + RB13 \cdot (\vec{b_{6,13}} \times \hat{d}_{13})_x = 0
\end{aligned} \tag{6.15}
$$

$$
\begin{aligned}
&(M_y + \vec{b_{6,9}} F_y) + RB7x \cdot (\vec{b_{6,7}} \times \hat{d}_{7a})_y + RB7y \cdot (\vec{b_{6,7}} \times \hat{d}_{7b})_y \\
&+ RB7z \cdot (\vec{b_{6,7}} \times \hat{d}_{7c})_y + RB12x \cdot (\vec{b_{6,12}} \times \hat{d}_{12a})_y + RB12y \\
&\cdot (\vec{b_{6,12}} \times \hat{d}_{12b})_y + RB12z \cdot (\vec{b_{6,12}} \times \hat{d}_{12c})_y + RB13 \cdot (\vec{b_{6,13}} \times \hat{d}_{13})_y = 0
\end{aligned} \tag{6.16}
$$

$$
\begin{aligned}
&(M_z + \vec{b_{6,9}} F_z) + RB7x \cdot (\vec{b_{6,7}} \times \hat{d}_{7a})_z + RB7y \cdot (\vec{b_{6,7}} \times \hat{d}_{7b})_z \\
&+ RB7z \cdot (\vec{b_{6,7}} \times \hat{d}_{7c})_z + RB12x \cdot (\vec{b_{6,12}} \times \hat{d}_{12a})_z + RB12y \\
&\cdot (\vec{b_{6,12}} \times \hat{d}_{12b})_z + RB12z \cdot (\vec{b_{6,12}} \times \hat{d}_{12c})_z + RB13 \cdot (\vec{b_{6,13}} \times \hat{d}_{13})_z = 0
\end{aligned} \tag{6.17}
$$

Force equilibrium equations for the lower platform:

$$
-(RB6x \cdot \hat{d}_{6ax} + RB6y \cdot \hat{d}_{6bx} + RB6z \cdot \hat{d}_{6cx} + RB13 \cdot \hat{d}_{13x}) + K_{4x} \cdot s_{4x} + K_{3x} \cdot s_{3x} + RC \cdot \hat{d}_{cx} = 0 \tag{6.18}
$$

$$-(RB6x \cdot \hat{d}_{6ay} + RB6y \cdot \hat{d}_{6by} + RB6z \cdot \hat{d}_{6cy} + RB13 \cdot \hat{d}_{13y}) + K_{4y} \cdot s_{4y} + K_{3y} \cdot s_{3y} + RC \cdot \hat{d}_{cy} = 0 \tag{6.19}$$

$$-(RB6x \cdot \hat{d}_{6az} + RB6y \cdot \hat{d}_{6bz} + RB6z \cdot \hat{d}_{6cz} + RB13 \cdot \hat{d}_{13z}) + K_{4z} \cdot s_{4z} + K_{3z} \cdot s_{3z} + RC \cdot \hat{d}_{cz} = 0 \tag{6.20}$$

Moment equilibrium equations for the lower platform about P4:

$$\begin{aligned} &RB13 \cdot (\vec{b_{4,18}} \times -\hat{d}_{13})_x + RB6x \cdot (\vec{b_{4,6}} \times -\hat{d}_{6a})_x + RB6y \cdot (\vec{b_{4,6}} \times -\hat{d}_{6b})_x \\ &+ RB6z \cdot (\vec{b_{4,6}} \times -\hat{d}_{6c})_x + K_{3x} \cdot s_{3x} \cdot (\vec{b_{4,3}} \times \hat{d}_{3a})_x + K_{3y} \cdot s_{3y} \\ &\cdot (\vec{b_{4,3}} \times \hat{d}_{3b})_x + K_{3z} \cdot s_{3z} \cdot (\vec{b_{4,3}} \times \hat{d}_{3c})_x + RC \cdot (\vec{b_{4,56}} \times \hat{d}_c)_x = 0 \end{aligned} \tag{6.21}$$

$$\begin{aligned} &RB13 \cdot (\vec{b_{4,18}} \times -\hat{d}_{13})_y + RB6x \cdot (\vec{b_{4,6}} \times -\hat{d}_{6a})_y + RB6y \cdot (\vec{b_{4,6}} \times -\hat{d}_{6b})_y \\ &+ RB6z \cdot (\vec{b_{4,6}} \times -\hat{d}_{6c})_y + K_{3x} \cdot s_{3x} \cdot (\vec{b_{4,3}} \times \hat{d}_{3a})_y + K_{3y} \cdot s_{3y} \\ &\cdot (\vec{b_{4,3}} \times \hat{d}_{3b})_y + K_{3z} \cdot s_{3z} \cdot (\vec{b_{4,3}} \times \hat{d}_{3c})_y + RC \cdot (\vec{b_{4,56}} \times \hat{d}_c)_y = 0 \end{aligned} \tag{6.22}$$

$$\begin{aligned} &RB13 \cdot (\vec{b_{4,18}} \times -\hat{d}_{13})_z + RB6x \cdot (\vec{b_{4,6}} \times -\hat{d}_{6a})_z + RB6y \cdot (\vec{b_{4,6}} \times -\hat{d}_{6b})_z \\ &+ RB6z \cdot (\vec{b_{4,6}} \times -\hat{d}_{6c})_z + K_{3x} \cdot s_{3x} \cdot (\vec{b_{4,3}} \times \hat{d}_{3a})_z + K_{3y} \cdot s_{3y} \\ &\cdot (\vec{b_{4,3}} \times \hat{d}_{3b})_z + K_{3z} \cdot s_{3z} \cdot (\vec{b_{4,3}} \times \hat{d}_{3c})_z + RC \cdot (\vec{b_{4,56}} \times \hat{d}_c)_z = 0 \end{aligned} \tag{6.23}$$

Force equilibrium equations for the camber link:

$$-(RB7x \cdot \hat{d}_{7ax} + RB7y \cdot \hat{d}_{7bx} + RB7z \cdot \hat{d}_{7cx}) + K_{1x} \cdot s_{1x} = 0 \tag{6.24}$$

$$-(RB7x \cdot \hat{d}_{7ay} + RB7y \cdot \hat{d}_{7by} + RB7z \cdot \hat{d}_{7cy}) + K_{1y} \cdot s_{1y} = 0 \tag{6.25}$$

$$-(RB7x \cdot \hat{d}_{7az} + RB7y \cdot \hat{d}_{7bz} + RB7z \cdot \hat{d}_{7cz}) + K_{1z} \cdot s_{1z} = 0 \tag{6.26}$$

Moment equilibrium equations for the camber link about P1:

$$RB7x \cdot (\vec{b_{1,7}} \times -\hat{d}_{7a})_x + RB7y \cdot (\vec{b_{1,7}} \times -\hat{d}_{7b})_x + RB7z \cdot (\vec{b_{1,7}} \times -\hat{d}_{7c})_x + M_1 \cdot d_{7bx} - M_{1x} = 0 \tag{6.27}$$

$$RB7x \cdot (\vec{b_{1,7}} \times -\hat{d}_{7a})_y + RB7y \cdot (\vec{b_{1,7}} \times -\hat{d}_{7b})_y + RB7z \cdot (\vec{b_{1,7}} \times -\hat{d}_{7c})_y + M_1 \cdot d_{7by} - M_{1y} = 0 \tag{6.28}$$

$$RB7x \cdot (\vec{b_{1,7}} \times -\hat{d}_{7a})_z + RB7y \cdot (\vec{b_{1,7}} \times -\hat{d}_{7b})_z + RB7z \cdot (\vec{b_{1,7}} \times -\hat{d}_{7c})_z + M_1 \cdot d_{7bz} - M_{1z} = 0 \tag{6.29}$$

Equation to constrain the zeta rotation along camber link:

$$M_1 - \zeta_1 \cdot K_{rot1}(y) = 0 \tag{6.30}$$

Force equilibrium equations for the toe link:

$$-(RB12x \cdot \hat{d}_{12ax} + RB12y \cdot \hat{d}_{12bx} + RB12z \cdot \hat{d}_{12cx}) + K_{14x} \cdot s_{14x} = 0 \tag{6.31}$$

$$-(RB12x \cdot \hat{d}_{12ay} + RB12y \cdot \hat{d}_{12by} + RB12z \cdot \hat{d}_{12cy}) + K_{14y} \cdot s_{14y} = 0 \tag{6.32}$$

$$-(RB12x \cdot \hat{d}_{12az} + RB12y \cdot \hat{d}_{12bz} + RB12z \cdot \hat{d}_{12cz}) + K_{14z} \cdot s_{14z} = 0 \tag{6.33}$$

Moment equilibrium equations for the toe link about P14:

$$\begin{aligned} &RB12x \cdot (\vec{b_{14,12}} \times -\hat{d}_{12a})_x + RB12y \cdot (\vec{b_{14,12}} \times -\hat{d}_{12b})_x \\ &+ RB12z \cdot (\vec{b_{14,12}} \times -\hat{d}_{12c})_x + M_{14} \cdot d_{12bx} - M_{14x} = 0 \end{aligned} \tag{6.34}$$

$$\begin{aligned} &RB12x \cdot (\vec{b_{14,12}} \times -\hat{d}_{12a})_y + RB12y \cdot (\vec{b_{14,12}} \times -\hat{d}_{12b})_y \\ &+ RB12z \cdot (\vec{b_{14,12}} \times -\hat{d}_{12c})_y + M_{14} \cdot d_{12by} - M_{14y} = 0 \end{aligned} \tag{6.35}$$

$$\begin{aligned} &RB12x \cdot (\vec{b_{14,12}} \times -\hat{d}_{12a})_z + RB12y \cdot (\vec{b_{14,12}} \times -\hat{d}_{12b})_z \\ &+ RB12z \cdot (\vec{b_{14,12}} \times -\hat{d}_{12c})_z + M_{14} \cdot d_{12bz} - M_{14z} = 0 \end{aligned} \tag{6.36}$$

Equation to constrain the zeta rotation along the toe link:

$$M_{14} - \zeta_{14} \cdot K_{rot14}(y) = 0 \tag{6.37}$$

Equation to constrain the spring displacement:

$$Rc - K_s \cdot s = 0 \tag{6.38}$$

Total 38 equations are formulated. New equilibrium position, force distribution and bushing deformations are obtained after solving these equations using a non linear solver.

7 Methodology for Sensitivity Analysis

The bushings in a suspension result in compliance in the system. It is important to select the stiffness values based on the elasto-kinematic requirements and targets and to meet isolation and comfort targets. Some of the parameters that are important in this study are:

- Brake force steer
- Lateral force steer
- Drive force steer
- Longitudinal, lateral and vertical compliance

When the vehicle is performing different driving manoeuvres, there will be changes in the kinematic parameters in the suspension system based on the compliance and the hardpoint setup. These changes to the parameters also influence the driving behaviour. For instance, during braking it is preferred that the vehicle has a toe out in the front and toe in configuration in the rear which helps in the braking stability. This can be achieved by a combination of different bushing stiffness in the system. A suspension system can comprise of many bushings ranging from 4 to 15 or more. Understanding the influence of each bushing on a particular parameter can be challenging due to the number of variables involved. Thus, sensitivity analysis can be performed to understand the effect of each bushing on a particular kinematic property. This will also help in the tuning process by allowing the design engineer to concentrate on the bushing which influences the most.

This analysis can be approached mathematically with the help of the linearized matrix as explained in section 2.8. Once the linearized matrix is obtained, it can be partially differentiated with respect to a design variable [2]. This will then yield the influence of that particular bushing stiffness on a performance variable.

$$\begin{bmatrix} -K_b \cdot \Delta_q \\ 0 \end{bmatrix} = \begin{bmatrix} K & \phi_q^T \\ \phi_q & 0 \end{bmatrix} \cdot \begin{bmatrix} \Delta q_b \\ \lambda_b \end{bmatrix} \tag{7.1}$$

The subscript 'b' in the above equation denotes the partial differentiation with respect to a particular design variable [2]. In this particular case the design variable 'b' is chosen as the bushing translation and the rotational stiffness of the different bushings in the system. In the above equation, K_b denotes the partial differentiation of the stiffness matrix with respect to the particular design variable. The performance variables are the above mentioned parameters like changes in toe and camber for a given lateral force or longitudinal force. After the sensitivity analysis, we obtain a matrix which denotes the effect of a bushing stiffness on the performance variable.

In the table 10.1, suspension parameters such as toe change, camber change, longitudinal, lateral & vertical displacements are tabulated for a vertical force of 5000N applied at the wheel contact point. The table illustrates the contribution of each bushing stiffness for a particular parameter change.

8 Methodology for Bushing stiffness Optimization

Sensitivity analysis determines the bushing which contributes significantly for a change in particular suspension parameter. Sensitivity analysis reduces the effort of optimising the bushing stiffness values to achieve certain suspension parameters. In this thesis work, multi-objective optimization tool is used to optimize the bushing stiffness values. When the suspension is in equilibrium, a force is applied at the wheel contact point. Certain suspension parameters are given as target values with bushing stiffness values as the variables. The multi-objective optimization tool tries to achieve the target values based on the weight values assigned to a particular parameter by varying the bushing stiffness values [2].

$$F(x) - \gamma \cdot weight \leq goal \tag{8.1}$$

Where, F(x) is a multi-objective function and this method finds the solution by converging the multi-objective function to a single objective function using a scalar variable γ. In the table below we can see few results from the optimization. We can see that the optimization tool tries to solve the system and adjusts the stiffness values in order to come as close as possible to the defined targets or the goal values.

The weight value of 0.1 is assigned to all the suspension parameters and the obtained solutions are shown in table 10.2 in the results section. The higher weight value can be assigned based on the the target which is of higher importance.

There are two different methods possible in the current optimization tool. The first one involves defining K and C targets when the wheel suspension system moves from one point to another. The second method involves optimizing the bushing stiffness when an external force acts on the system at equilibrium (once the suspension system has already moved). This generally involves very small displacements.

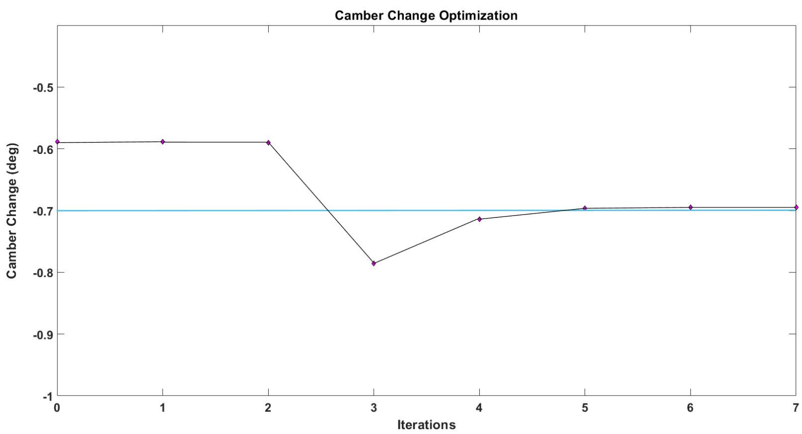

Figure 8.1: Target tracking for camber angle optimization

The figure 8.1 shows how the solver tries to reach the goal value defined by the user. The target was a camber goal of -0.7 deg. As the number of iterations increase the solver reaches the defined value by changing the bushing stiffness.

9 Modelling Suspension Systems in ADAMS Car

9.1 Building a suspension template

In order to verify the results from the mathematical model developed in MATLAB, the five link suspension system was modelled on MSC ADAMS Car. The following simplification were done in the ADAMS Car model in order to compare the results from both the models:

- There is no damping in the system and the damping force throughout the wheel movement is zero
- Linear bushing models are considered without any damping and the orientation of the bushing is similar as chosen in the MATLAB model
- The forces are applied at the tyre contact point and the wheel mass is considered to be as low as possible
- The links are rigid, massless and linear spring is considered
- The model can be analyzed in both compliant mode and purely kinematic mode

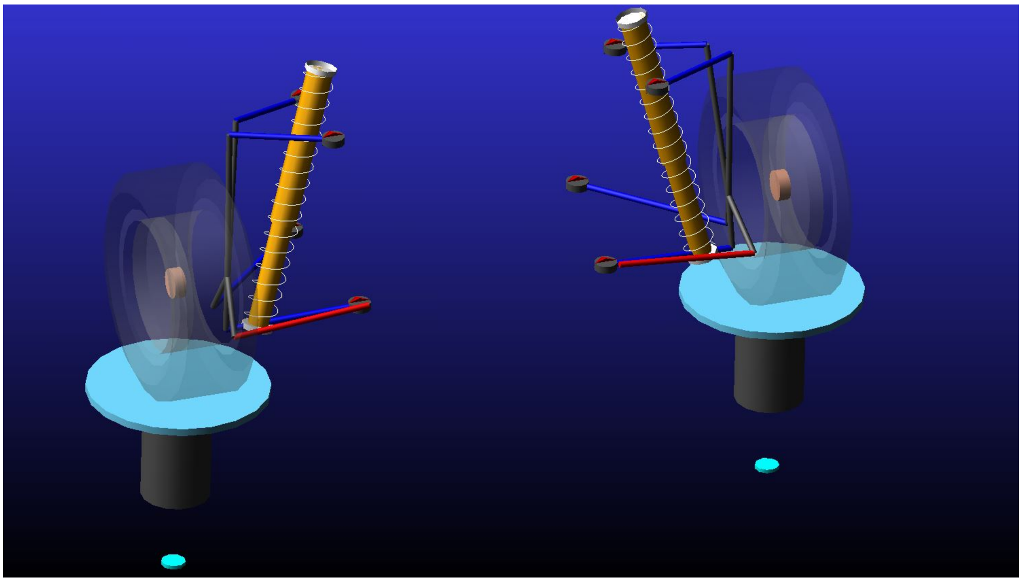

Figure 9.1: Five link suspension model in ADAMS Car

As we can see in the figure 9.1, the compliance is added in the model by introducing bushings at 4 points in the model with both translation and rotation stiffness.

The links are connected to the knuckle with the help of spherical joints and are connected to the subframe by a bushing. However, the steering link is connected to chassis side by a universal joint. The spring damper system is connected to the top mount by a universal joint and the lower mount is connected to the lower control arm by a spherical joint. The lower mount is also connected to the top mount by a translation joint.

The forces at different joint locations and the bushing deformations in the ADAMS Car model are compared with the mathematical model for varying vertical force, lateral force and longitudinal force on the tyre. In order to verify mathematical models for Integral link and four link suspension, similar templates are built.

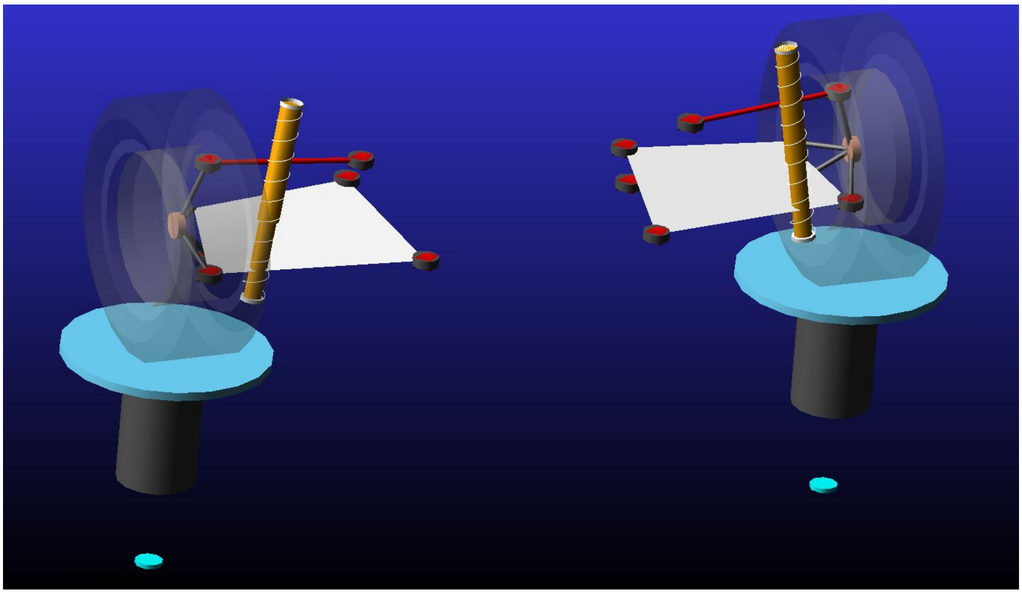

Figure 9.2: Integral link suspension model in ADAMS Car

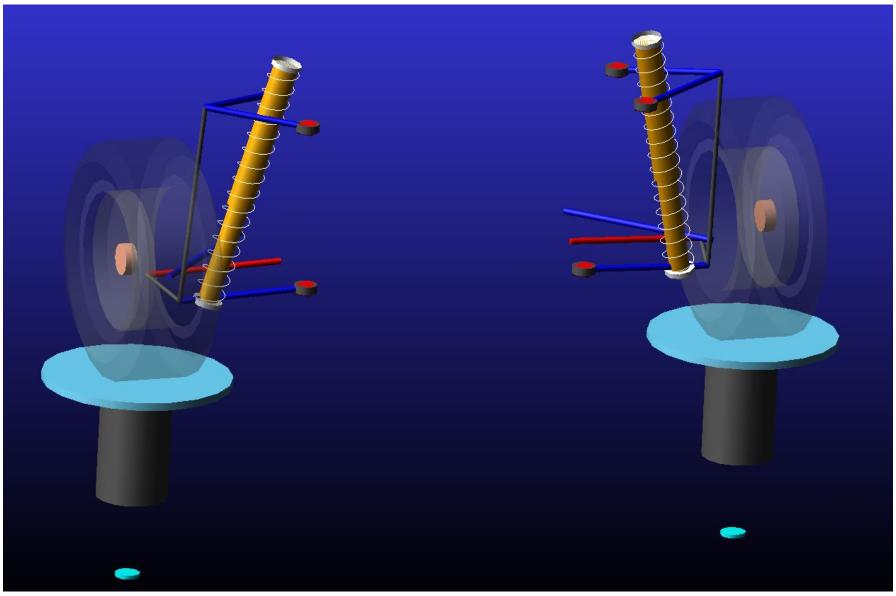

Figure 9.3: Four link suspension model in ADAMS Car

An important aspect that needs to be considered while verifying the results are the hub forces and moments. The hub forces and moments generated in the ADAMS Car model are a function of tyre radius, tyre stiffness and its weight. These parameters are modelled in the developed analysis tool. The hub moments needs to be considered for all simulations as they play a vital role in the force distribution at different joints.

10 Results and Discussions

As the mathematical model is getting built in stages, it becomes mandatory to verify the model after each stage to rectify any minor mistakes in the model. Some of the methods opted for the verification of the mathematical models are mentioned in this section and various results are also discussed.

10.1 Position Constraint

The mathematical model helps to determine the new equilibrium position for a wheel force input. A 3D plot is generated by joining the hardpoints in space to form links and knuckle. As the new equilibrium hardpoints are calculated from the model, these are plotted on the same 3D plot to observe the motion of the suspension.

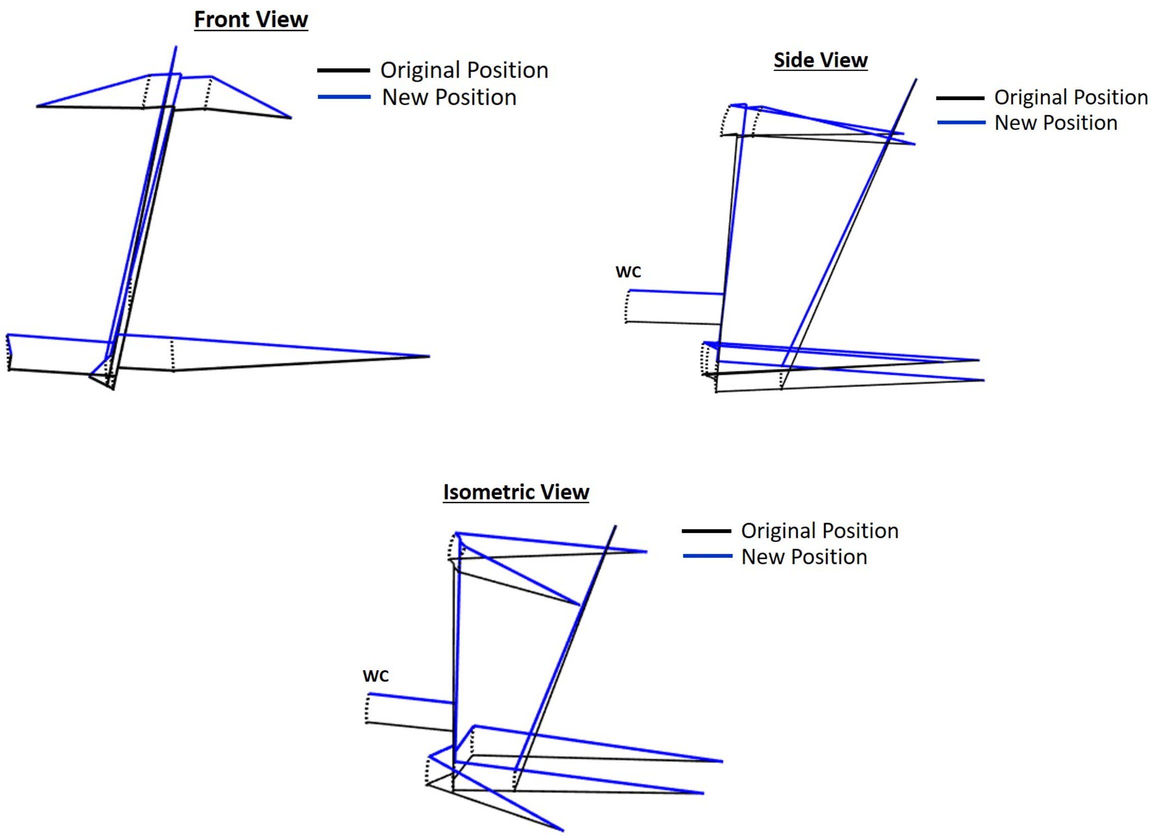

Figure 10.1: Depiction of suspension wheel travel

For example, a vertical force of 5kN is applied at the wheel center and figure 10.1 represents Wheel center movement in three different views. The black structure represents the initial position of the suspension and the blue structure represents the new equilibrium position after force is applied. The spring gets compressed by 48.63mm and the wheel center moves up by 68.82mm.

10.2 Verification of reaction forces and bushing deformations

The first step in verification is comparison of results from the mathematical model and the ADAMS Car model. This verification will help in understanding the established methodology and the nature of the results. A vertical force of 1600N is applied at the tyre contact point of the five link suspension system and the force distribution at the different links are compared.

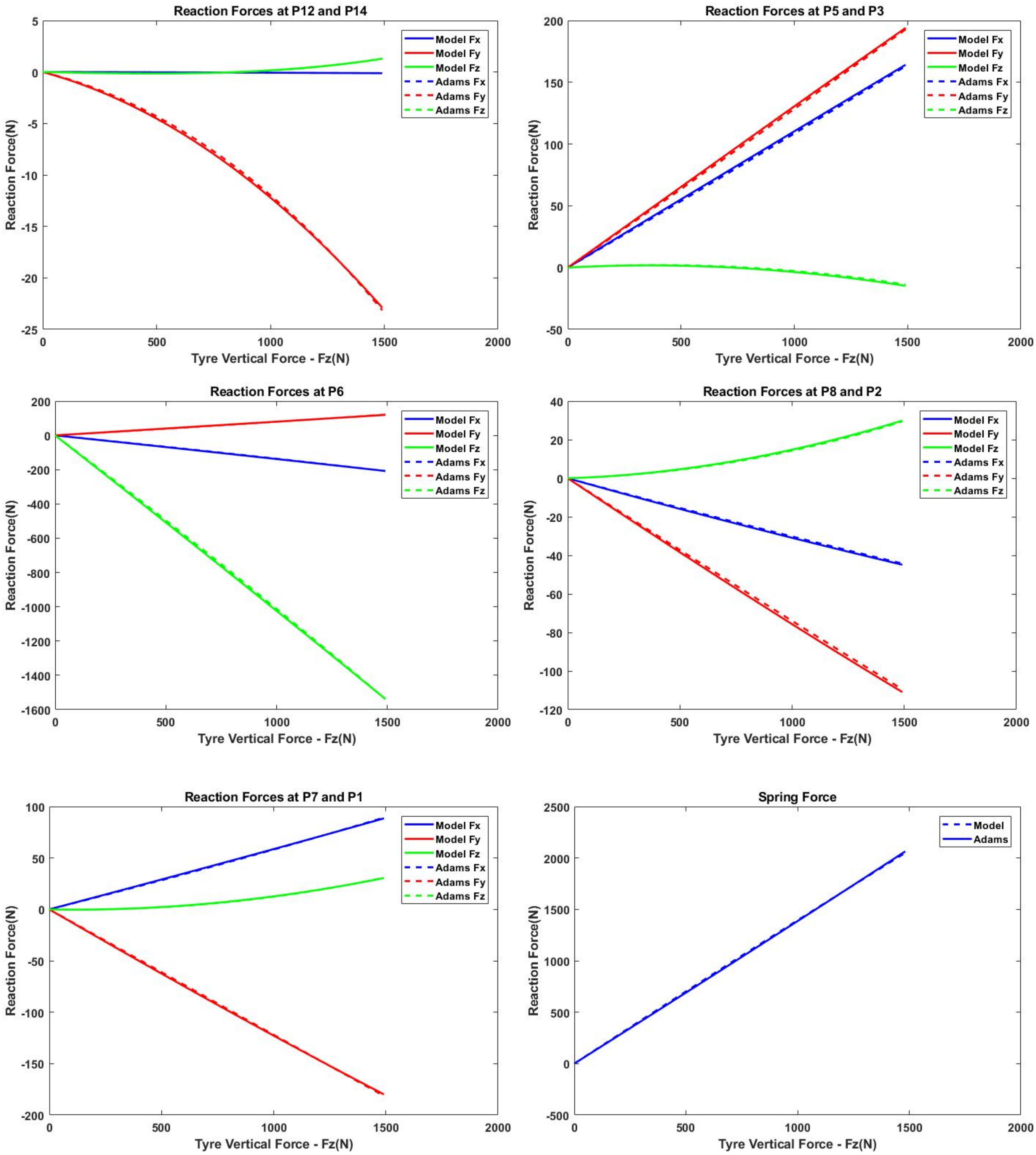

Figure 10.2: Comparison of reaction forces from the mathematical model and MSC ADAMS Car for vertical wheel loads

In the plots above, F_x, F_y, F_z denote the forces in the x, y and z directions respectively. From the above we can see that there is a good match in results between both the models.

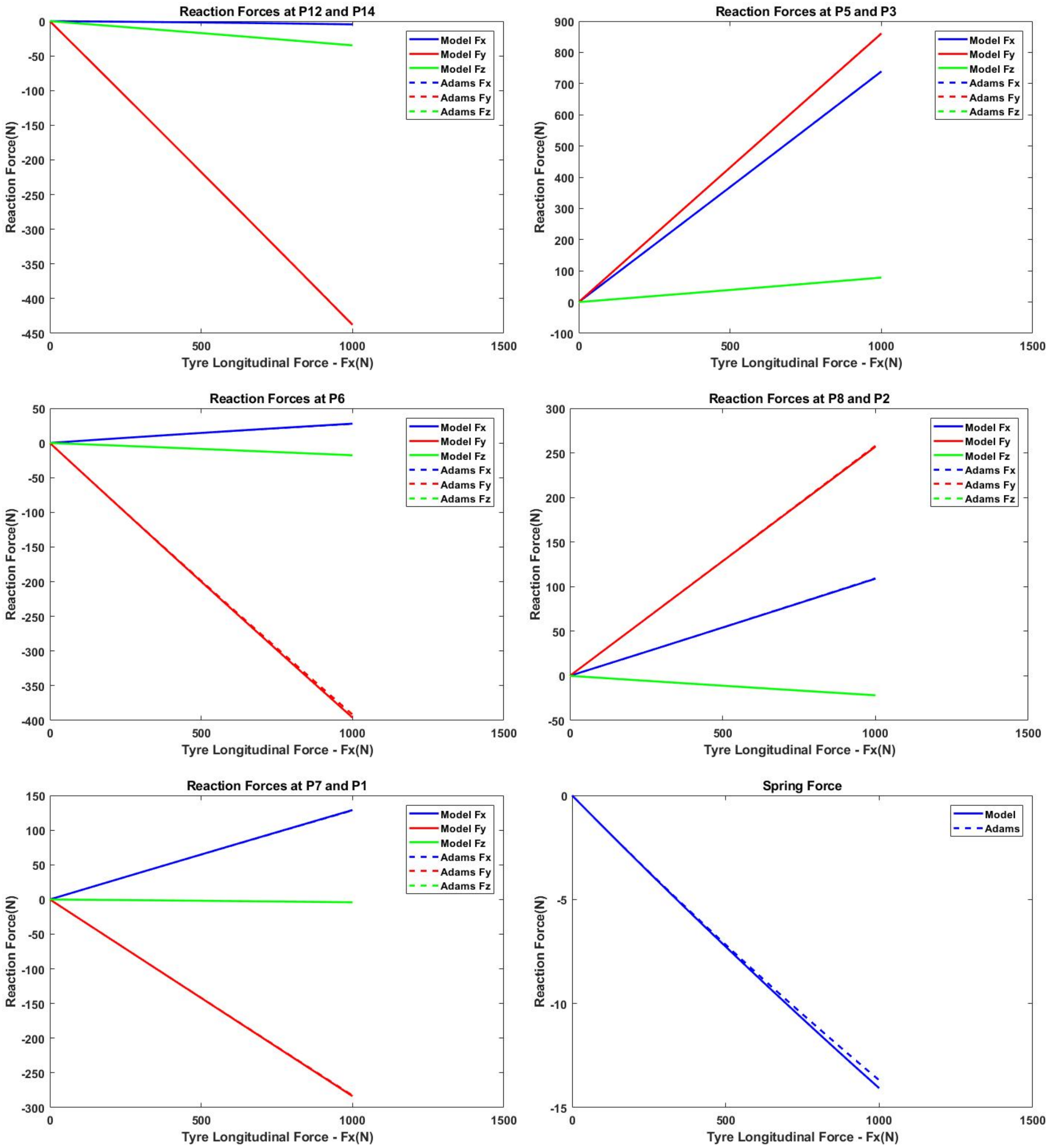

Figure 10.3: Comparison of reaction forces from the mathematical model and MSC ADAMS Car for longitudinal wheel loads

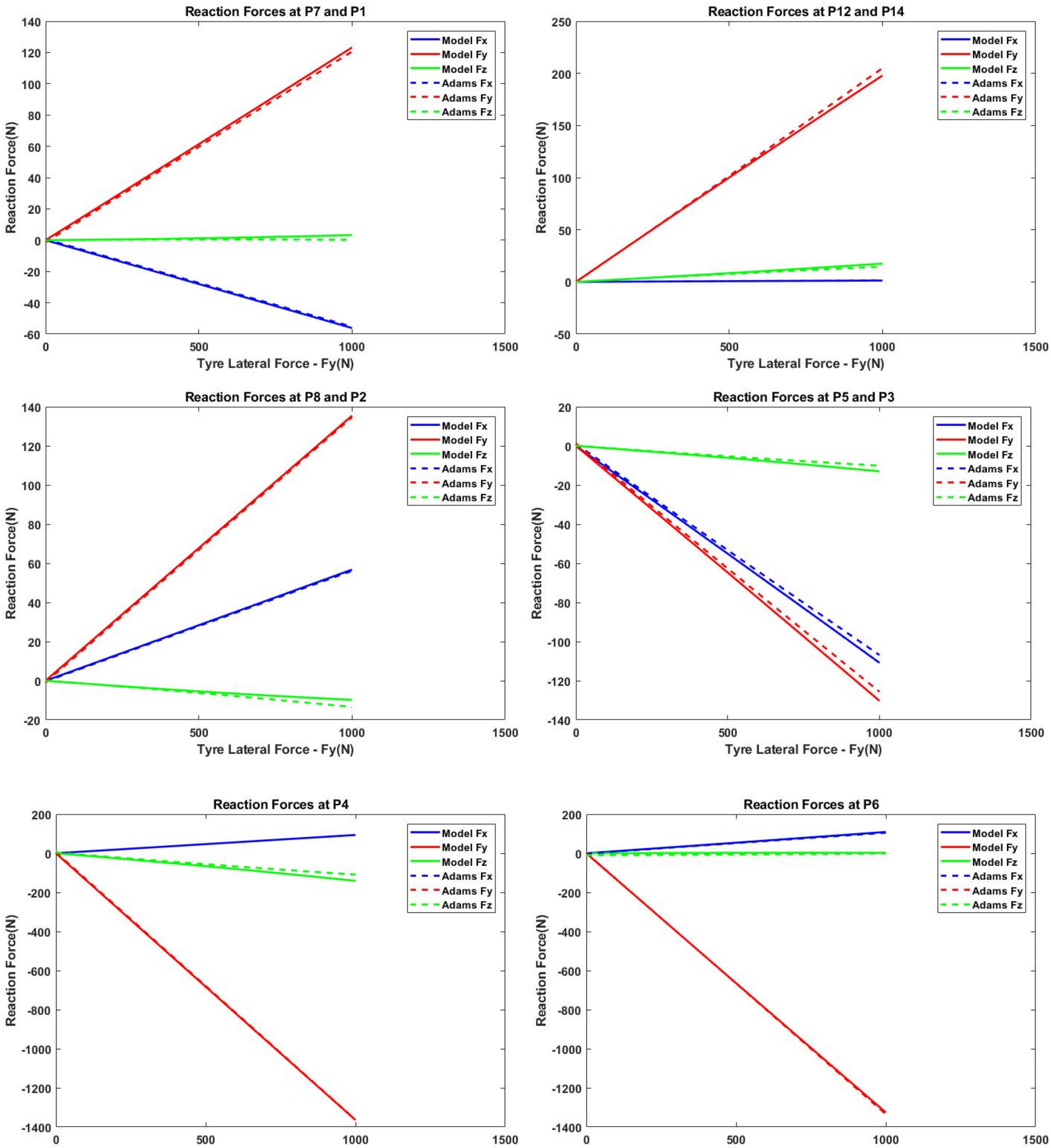

Figure 10.4: Comparison of reaction forces from the mathematical model and MSC ADAMS Car for Lateral wheel loads

The above plots shows that the reaction forces obtained from the mathematical model are almost the same when compared with Adams Car simulation results for all the applied external forces in x, y and z directions at the tyre contact point. The bushing deformations due to the external force applied can also be compared with the MSC ADAMS Car software. In the fig. 10.5, the terms s_x, s_y, s_z denote the bushing displacements in x, y and z directions respectively. The results indicate a very good match between the developed model and the results from

ADAMS.

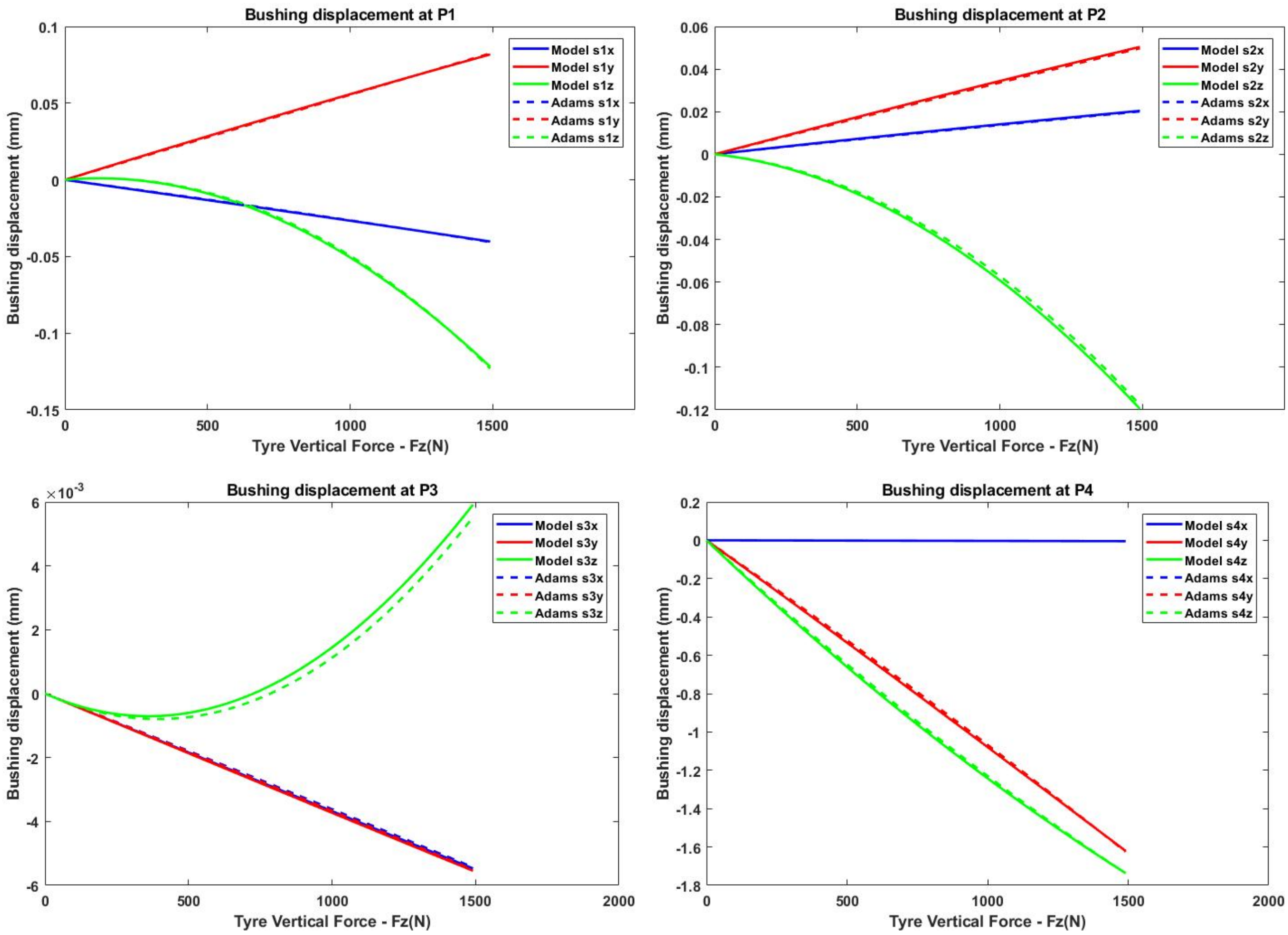

Figure 10.5: Comparison of bushing displacements from the mathematical model and MSC ADAMS Car for vertical wheel loads

10.3 Kinematic and Compliance analysis

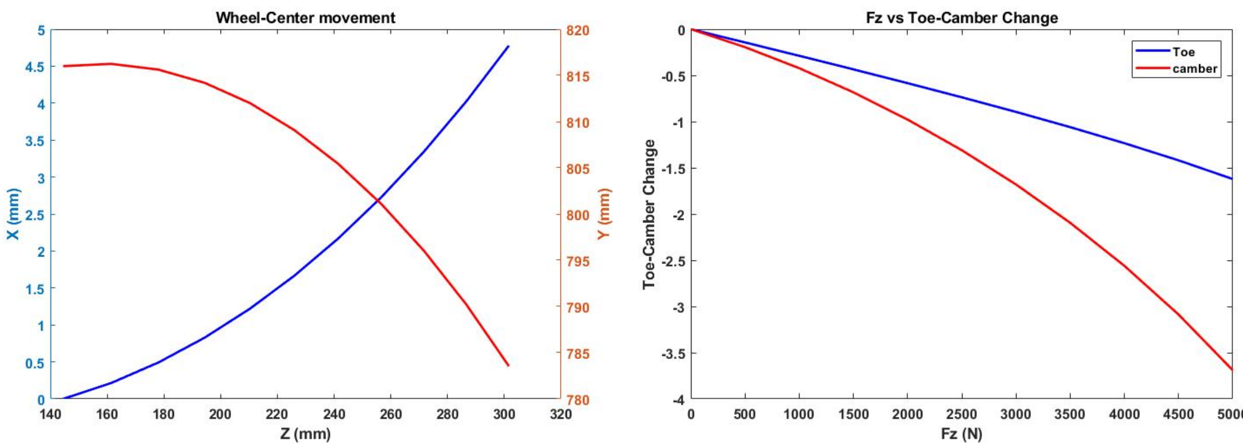

Figure 10.6: Wheel-Center Movement and Toe-Camber Change

Figure 10.6 represents the wheel center movement and the toe camber change due to vertical force. The movement of the wheel center in Y direction increases, reaches to the maximum value and then decreases as the wheel moves further up in the Z direction.

Initially, the toe and camber are assumed to be zero in order to study the change in these parameters. When the vertical force is applied, in the toe-camber change plot, At Fz=0 the toe is around 0.04 deg and camber is around -0.09 deg. This is due to the wheel-carrier weight which is assumed to be 30kg. The toe change and the camber change can be seen decreasing as Fz increases which means as the vertical force is applied, the obtained jounce influences toe-in and negative camber gain conditions.

The analytical tool also helps to trace the movements of different hardpoints in the system. Below graphs show the comparison in movement of hardpoints for rigid and compliant joints for varying wheel vertical force (Fz).

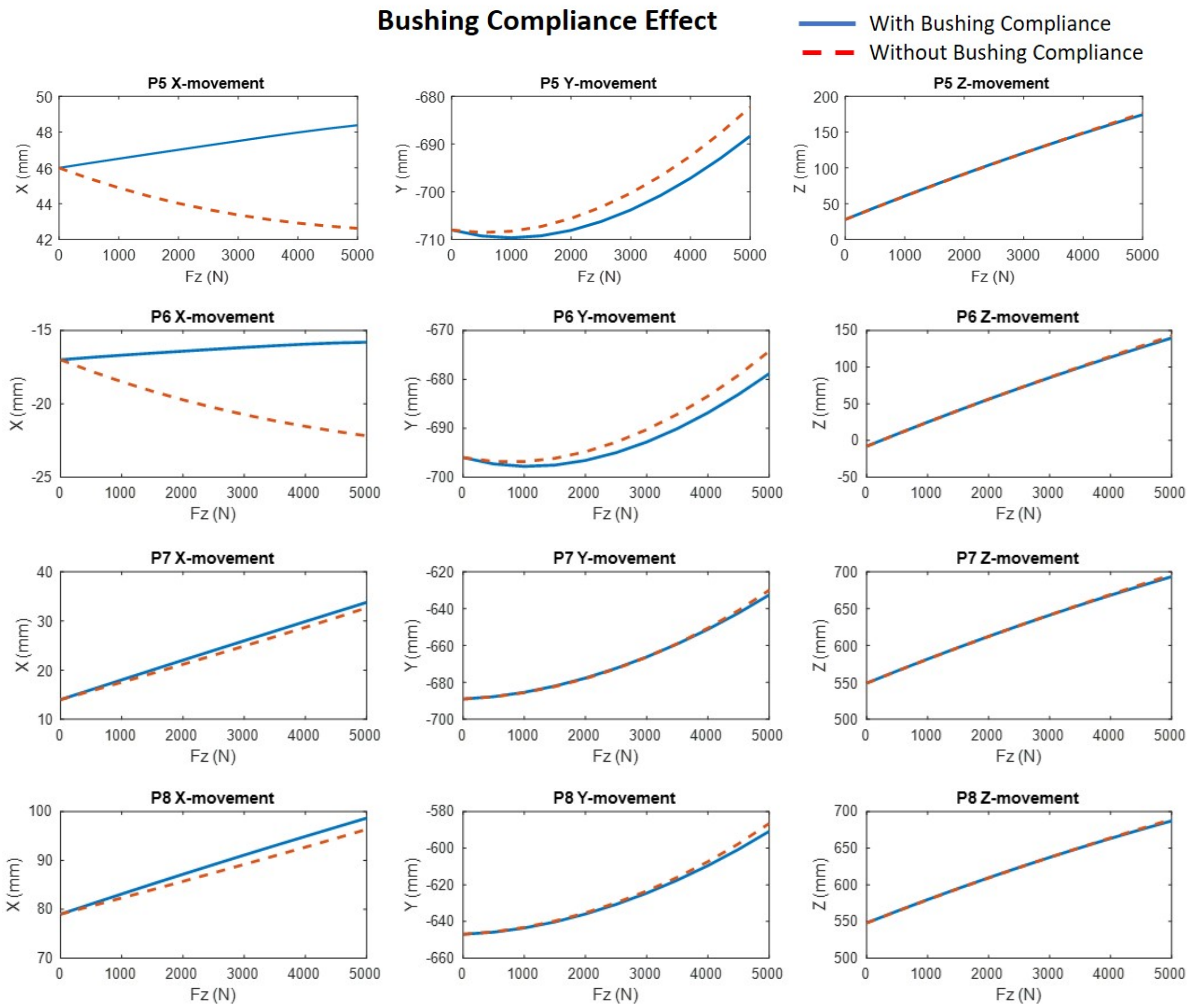

Figure 10.7: Comparison of bushing displacements from the mathematical model and MSC ADAMS for vertical wheel loads

In the figure 10.8, the same range of forces are applied as in case of rigid body study shown in figure 10.6. It can be seen that the implementation of bushings has affected the wheel center movement and the toe-camber angle change values due to the compliance. These values depend on the bushing stiffness and the orientations of the bushings in global coordinate system.

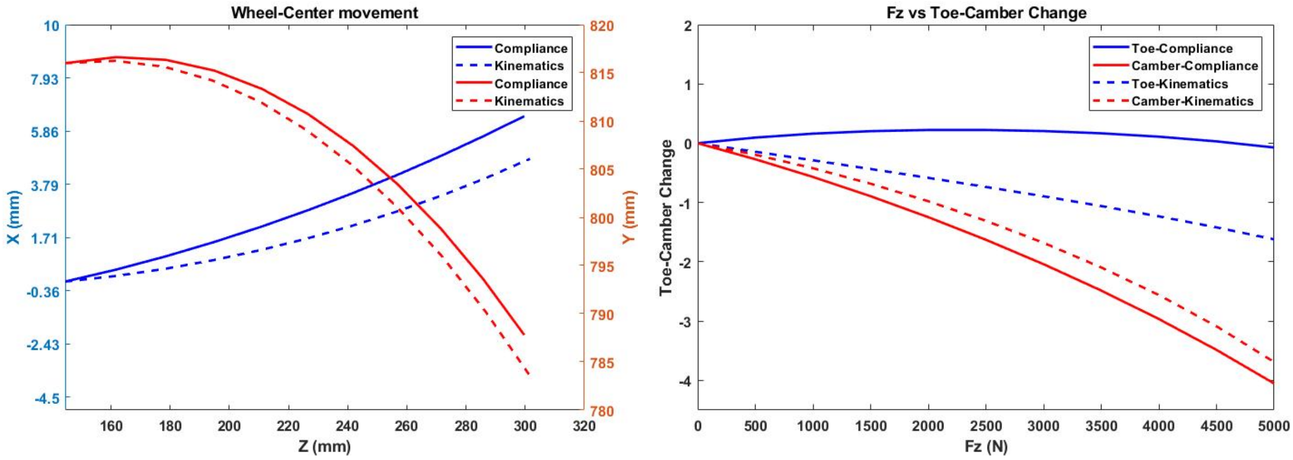

Figure 10.8: Wheel center movement and Toe-Camber change with compliance

Thus, the tool can be effectively used in elastokinematic analysis. The tool can accurately predict the force distribution at different joints and the model can be simulated for both kinematic and compliant setups. The tool presents the design engineer with a lot of information about the elastokinematic properties of the system at a very early phase in the suspension concept development phase.

10.4 Model verification for Integral link suspension system

As discussed earlier the methodology is implemented for an Integral link and a four link suspension system. The results for the join reaction between the developed mathematical and MSC ADAMS Car model are compared. It is found that both the results have a very good match. Thus the established methodology can provide reliable results in elastokinematic analysis.

Following are the results for the implementation of bushings on the knuckle side:

- In the mathematical model it is assumed that the forces on the ends of the link are equal. For instance, when a bushing is implemented on the knuckle side, the mathematical model calculates the reaction forces such that they are equal at P7 and P1 for bushings at both P7 and P1
- However, this is not the case in case of the ADAMS model. The forces at the ends of the link are not equal when both the points have bushings. The variation in force was seen only along the z direction and the difference in magnitude was less than 70N. This can be further evaluated in future work
- Thus the assumption that the force at both the ends of the link are equal can still produce reliable results and does not deviate too much when compared with ADAMS Car simulation results

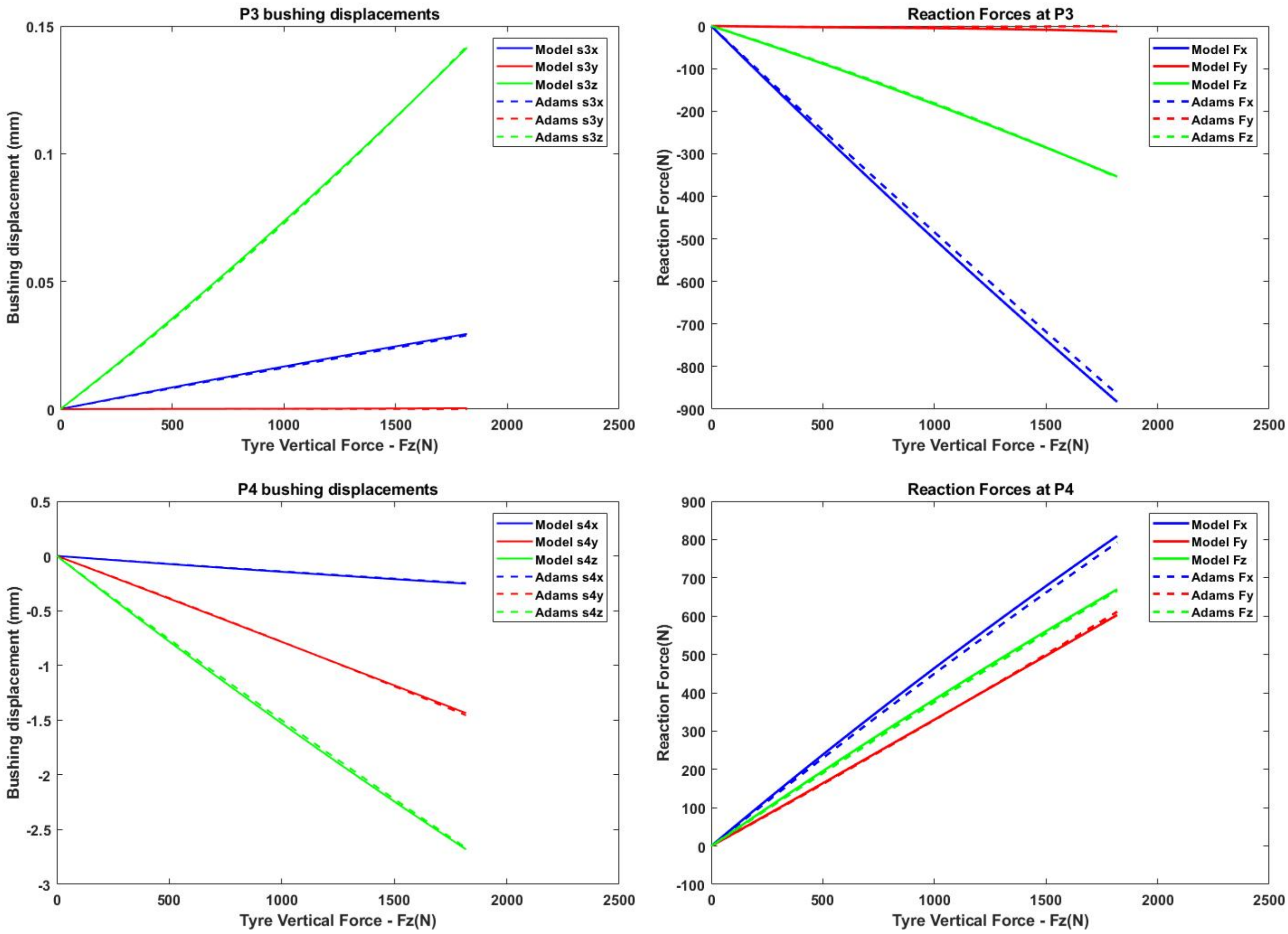

Figure 10.9: Comparison of bushing displacements from the mathematical model and MSC ADAMS Car for vertical wheel loads

The established methodology for the Integral link suspension system shows a good match in results when compared with simulations in MSC ADAMS Car. The methodology can further be applied to other complex suspension systems which can aid in elastokinematic analysis.

10.5 Sensitivity analysis

A suspension system (for one wheel) can comprise of 5 to 10 bushings or more. Each bushing has a total of 6 parameters (3 translation and 3 rotation stiffness), thus the number of variables can range from 30 - 60 and can make tuning complex. With the help of sensitivity analysis it is easier to focus on critical bushing variables which influence the K&C parameter the most.

The table below shows results from this analysis when 4 bushings are implemented in the current 5 link suspension system. The analysis was carried out for a vertical force of 5000N acting at the wheel contact point. The performance variable (brake steer, lateral compliance and so on) can be chosen as per the requirements and the design variables are the bushing parameters. As the force is applied at the wheel contact point, the suspension system attains new equilibrium position and the deflection from initial positions are determined. It can be observed from the table that the bushing variables $K4y$, $K4z$, $K1y$, $K1z$, $K2y$, $K2z$ are more sensitive to the performance variables. Thus, the design engineer can now focus on these bushings and tune easily, rather than considering all the variables. The variables contributing the most are highlighted in red in the table below.

Bushings	Stiffness Values (N/mm or Nmm/rad)	Toe angle change (deg) by Fz	Camber angle change (deg) by Fz	Longitudinal deflection (mm) by Fz	Lateral deflection (mm) by Fz	Vertical deflection (mm) by Fz
		5000N	**5000N**	**5000N**	**5000N**	**5000N**
K3x	30000	0.0000177	0.0000106	0.0004806	0.0000447	-0.0000821
K3y	35000	0.0000200	0.0000120	0.0005429	0.0000505	-0.0000928
K3z	2500	0.0000214	0.0000128	0.0005827	0.0000542	-0.0000994
K3rx	16000	0.0000003	0.0000002	0.0000001	0.0000004	-0.0000021
K3ry	3000	0.0000019	0.0000010	0.0000014	0.0000023	-0.0000148
K3rz	3000	0.0000232	0.0000063	-0.0000298	0.0000344	-0.0000299
K4x	3200	-0.0001732	0.0007746	0.0053534	-0.0023759	-0.0021522
K4y	420	-0.0059224	0.0265140	0.1832100	-0.0813130	-0.0736770
K4z	250	-0.0000002	0.0000005	0.0000038	-0.0000018	-0.0000009
K4rx	16000	0.0000011	0.0000005	-0.0000005	0.0000017	-0.0000111
K4ry	3000	0.0000012	0.0000006	-0.0000006	0.0000020	-0.0000124
K4rz	3000	0.0000047	-0.0000023	-0.0000492	0.0000183	0.0000038
K1x	2200	-0.0003915	0.0010075	-0.0043698	-0.0023122	-0.0017962
K1y	2200	-0.0024977	0.0064163	-0.0277900	-0.0147380	-0.0114390
K1z	250	-0.0021087	0.0054020	-0.0234190	-0.0124200	-0.0095898
K1rx	5500	0.0000026	0.0000034	-0.0000003	0.0000000	-0.0000332
K1ry	5500	0.0000010	0.0000005	-0.0000035	0.0000016	-0.0000062
K1rz	5500	0.0000133	-0.0000044	-0.0000928	0.0000433	0.0000066
K2x	2200	0.0000644	0.0000182	-0.0000684	0.0000879	-0.0000036
K2y	2200	0.9894900	0.2942600	-0,0010782000	0,0013962000	-0,0010820000
K2z	250	0.2940300	0.2233000	-0.5744900	0.8317800	-0,0096399000
K2rx	5500	0.0000065	0.0000040	-0.0000106	0.0000153	-0.0001439
K2ry	5500	0.0000005	0.0000002	-0.0000006	0.0000008	-0.0000039
K2rz	5500	0.0000207	0.0000059	-0.0000245	0.0000296	-0.0000273

Table 10.1: Sensitivity study on four bushings at P1, P2, P3 & P4

10.6 Bushing stiffness optimization and target tracking

The results from the optimization are shown below. The goal values are defined based on K and C requirements. We can see that the solver tries to come as close as possible to the goal values and uses the least square quadratic programming method in solving this multi objective optimization problem.

Suspension Paramters	Initial Values	Goal values	Weight values	Achieved Values
Toe change (deg)	0,16601	0,6	0.1	0,58619
Camber change (deg)	-0,58899	-0,9	0.1	-0,73125
Horizontal Displacement (mm)	0,91334	1,2	0.1	1,3708
Lateral Displacement (mm)	-0,30845	-0,8	0.1	-0,95
Vertical Displacement (mm)	34,323	35	1	34,816

Table 10.2: Optimization results

In order to answer the question on how the solver tracks the targets, the below table provides some insights on the same. In the table 10.3 the initial and the optimized bushing stiffness values for four bushings are listed. The solver tries to attain the defined goal values by changing the bushing stiffness parameters under the defined set of constraints.

	Initial stiffness	Optimized stiffness		Initial stiffness	Optimized stiffness
$Kb3_x$	30000	30000	$Kb1_x$	2200	2199.8
$Kb3_y$	35000	35000	$Kb1_y$	2200	2199.3
$Kb3_z$	2500	2500	$Kb1_z$	250	249.81
$Kb3_{rx}$	16000	16000	$Kb1_{rx}$	5500	5501.1
$Kb3_{ry}$	3000	3000.4	$Kb1_{ry}$	5500	5500.2
$Kb3_{rz}$	3000	3000	$Kb1_{rz}$	5500	5500
$Kb4_x$	3200	3200	$Kb2_x$	2200	2199.9
$Kb4_y$	420	63.652	$Kb2_y$	2200	2199.5
$Kb4_z$	250	274.47	$Kb2_z$	250	249.72
$Kb4_{rx}$	16000	16001	$Kb2_{rx}$	5500	5501.5
$Kb4_{ry}$	3000	3000.1	$Kb2_{ry}$	5500	5500.2
$Kb4_{rz}$	3000	3000	$Kb2_{rz}$	5500	5500

Table 10.3: Bushing stiffness optimization

Thus, these tools and methods of analysis are very effective for the design engineer during the concept study and provide more information on the elasto-kinematic properties of the system.

11 Deliverables and conclusions

From the above description of the methodology and the results it can be seen that the tool can be widely used for suspension elasto-kinematic and purely kinematic analysis. The applications of the analysis tool can help the design engineer by providing more data on the elastokinematic properties of the suspension system during the suspension concept development phase.

There are mainly 2 methodologies that have been explored in this thesis work. Both the methodologies can produce robust results but have few differences in the modelling approach. The methodology described in chapter 4 can be easier for implementation and to completely constrain the system by matching the number of unknowns and equations without the need of introducing extra equations. The methodology has been successfully applied for a Four link, Five link and an Integral link suspension system. The results from the analysis tool have a close to perfect match with the results from MSC ADAMS Car.

The analysis tool can also help to focus on critical design parameters during the tuning process with features like Sensitivity Analysis and Multi Objective Optimization. The above analysis will help the design engineer to focus on the important design parameters which has the highest influence on a particular Kinematic and Compliance parameter. The multi objective optimization was also seen to be very effective. For different combinations of toe and camber angles, the solver was successful in achieving the target values by changing the bushing stiffness values. This can significantly help in reducing the time taken during the tuning process.

The mathematical models are solved by using non linear solvers in MATLAB. It was observed that the solver algorithm also plays a vital role. Thus, it is important to choose the right solver setup and tolerance values for accurate solutions. For a system with well defined constraints, the solver is not very sensitive to the initialized values and can still converge rapidly towards the solution.

A GUI has been developed for the tool and the following features are provided which will aid in elastokinematic analysis and also allow the design engineer to easily work with the tool:

- Tracking of hardpoints and suspension movement under different configurations
- Elasto-kinematic analysis and possibility to modify bushing stiffness and orientation
- Predict force distribution at different joints in the system
- Perform sensitivity analysis
- Bushing stiffness optimization to reach defined goals
- Visualization of suspension movement
- Select number of bushings in the system and options to simulate both kinematic and compliant modes

The implemented GUI on MATLAB App designer is shown in the figure below. It is a simple to use tool and makes it very easy for data post processing as well.

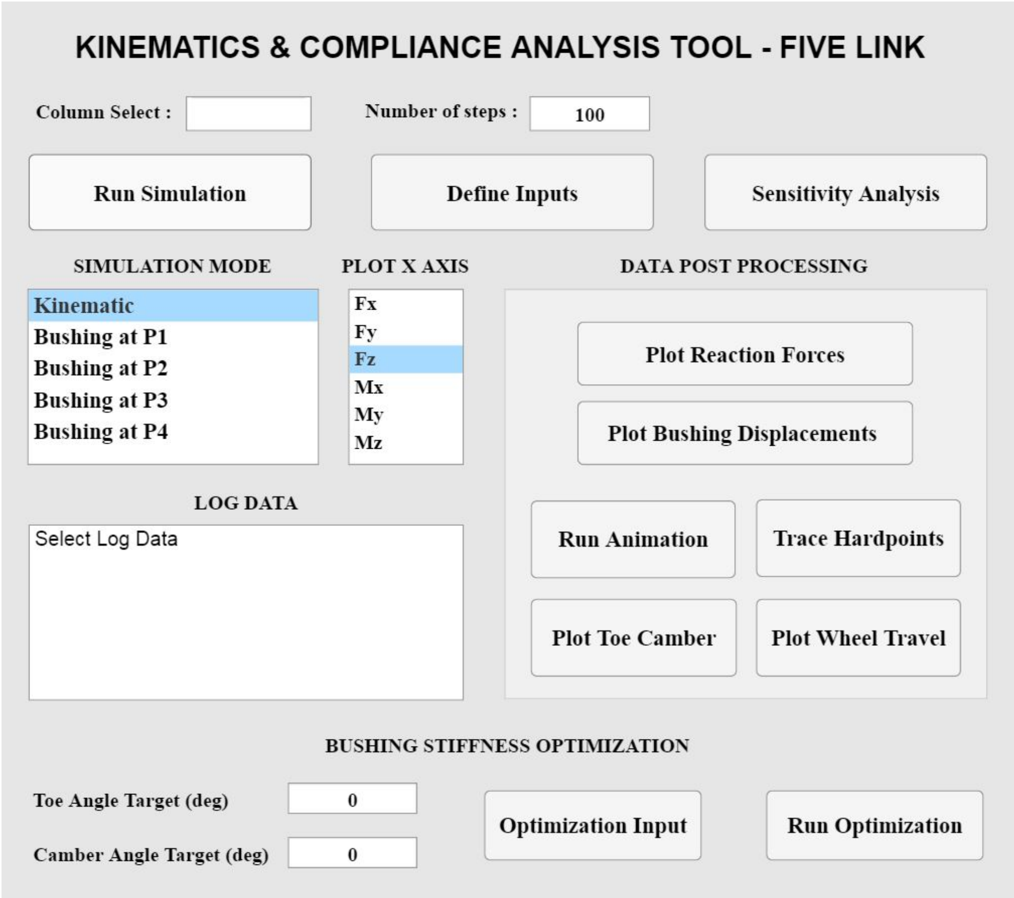

Figure 11.1: GUI for the Kinematics and Compliance Analysis Tool

12 Future work

Currently, the methodology for analysis of kinematics and compliance of a suspension system is established for a Five link suspension, a Four link suspension and an Integral link suspension system. This involves tools for tracking the wheel center movement under different wheel forces, sensitivity analysis to identify critical bushings and optimization technique to find optimum value of bushing stiffness.

As a scope for future work the research can be continued by :

- Implementation of non linear springs and bushing models
- Dynamic behaviour modelling
- Frequency response analysis
- Implementation of established methodology for other types of suspension systems
- Investigate the linear inverse relationship

13 References

[1] Rocca, E. and Russo, R., 2002. A feasibility study on elastokinematic parameter identification for a multilink suspension. Proceedings of the Institution of Mechanical Engineers, Part D: Journal of Automobile Engineering, 216(2), pp.153-160.

[2] Kang, J.S., Yun, J.R., Lee, J.M. and Tak, T.O., 1997. Elastokinematic analysis and optimization of suspension compliance characteristics. SAE transactions, pp.87-93.

[3] Knapczyk, J. and Dzierz˙ ek, S., 1995. Displacement and force analysis of five-rod suspension with flexible joints.

[4] Kang, J.S., Bae, S., Lee, J.M. and Tak, T.O., 2003. Force equilibrium approach for linearization of constrained mechanical system dynamics. J. Mech. Des., 125(1), pp.143-149.

[5] Blundell, M. and Harty, D., 2004. Multibody systems approach to vehicle dynamics.

[6] Huang, Yansong 2018, Knowledge and Requirements based Wheel Suspension Template, Stuttgart University, Germany.

[7] Henderson, D.M., 1977. Shuttle Program. Euler angles, quaternions, and transformation matrices working relationships.

[8] Chappuis, D., 2013. Constraints Derivation for Rigid Body Simulation in 3D.

[9] Nikravesh, P. E., Haug, E. J. (1983). Generalized coordinate partitioning for analysis of mechanical systems with nonholonomic constraints.

[10] Tang, L., Shangguan, W. B., Dai, L. (2012). A calculation method of joint forces for a suspension considering nonlinear elasticity of bushings. Proceedings of the Institution of Mechanical Engineers, Part K: Journal of Multi-body Dynamics, 226(4), 281-297.

[11] Caputo, A., Spina, M., Guglielmino, E. (2003). Sensitivity of Suspension System Performance to Bushing Stiffness Variation-An Evaluation Methodology. SAE transactions, 166-177.

[12] Andrea Trivella.(2015). Numerical modelling and simulation. Technical report, Politecnico di Torino.